



Support:



Nanoplasmonics: Optical Properties of Plasmonic Nanosystems

Mark I. Stockman

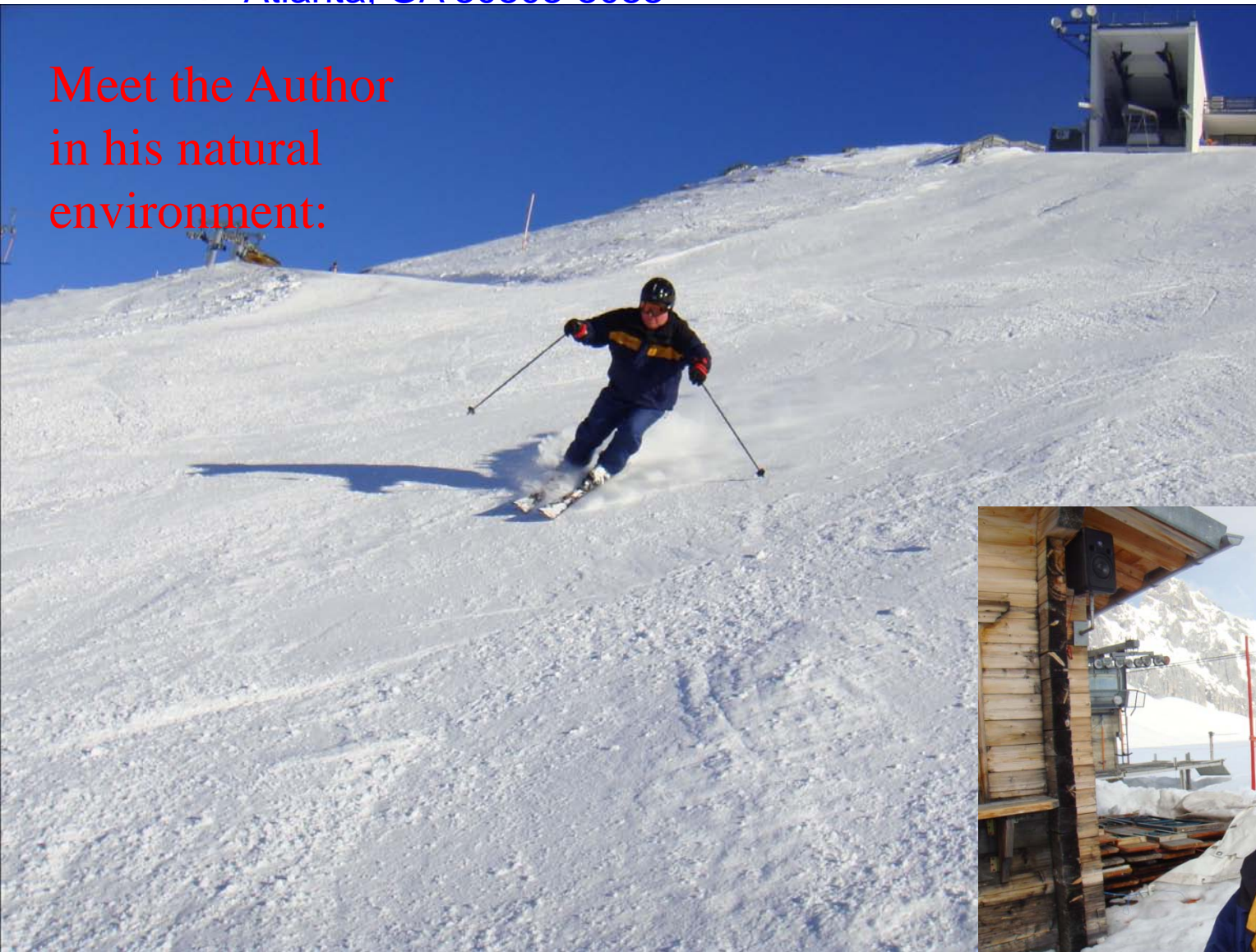
Department of Physics and Astronomy, Georgia
State University, Atlanta, GA 30303, USA

Lecture 1:

Introduction to Nanoplasmonics.

**Plasmon Polaritonics: Propagation of Surface
Plasmon Polaritons in Nanostructured Systems**

Meet the Author
in his natural
environment:



CONTENTS OF THE COURSE

- **Lecture 1: Introduction to Nanoplasmonics. Plasmon Polaritonics: Propagation of Surface Plasmon Polaritons in Nanostructured Systems**
- **Lecture 2: Nanoplasmonics of Nanosystems: Localized Surface Plasmon Resonances**
- **Lecture 3: Ultrafast, Nonlinear, and Quantum Nanoplasmonics**

LECTURE 1

Introduction to Nanoplasmonics.

Plasmon Polaritonics: Propagation of Surface Plasmon Polaritons in Nanostructured Systems

1. Introduction

Problem of nanolocalization of energy

Surface plasmons and enhanced optical fields

Applications of surface plasmonics

2. Surface plasmon polaritons as interface electromagnetic waves

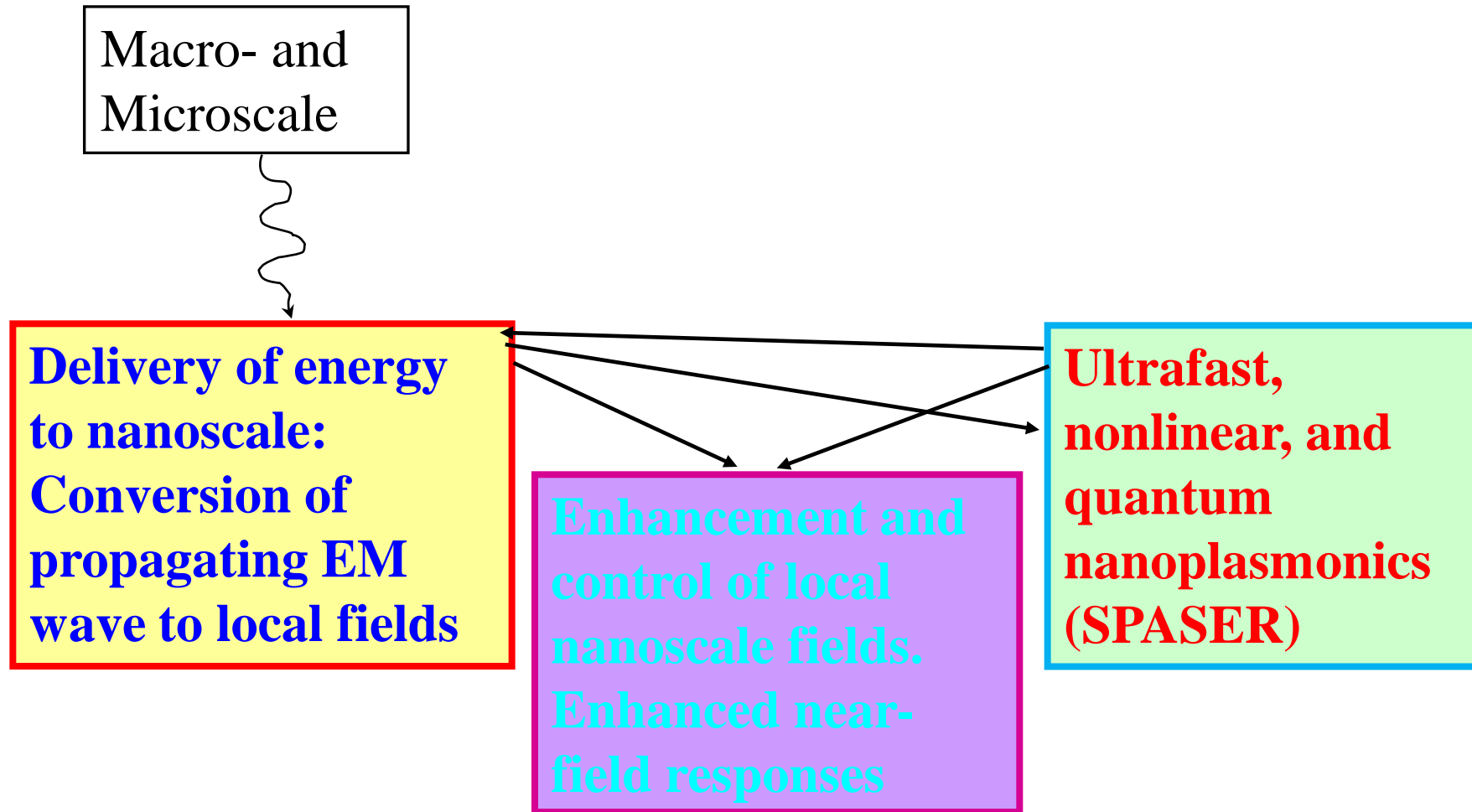
Maxwell equations solution for metal-dielectric interface

Surface plasmon polaritons in layered media

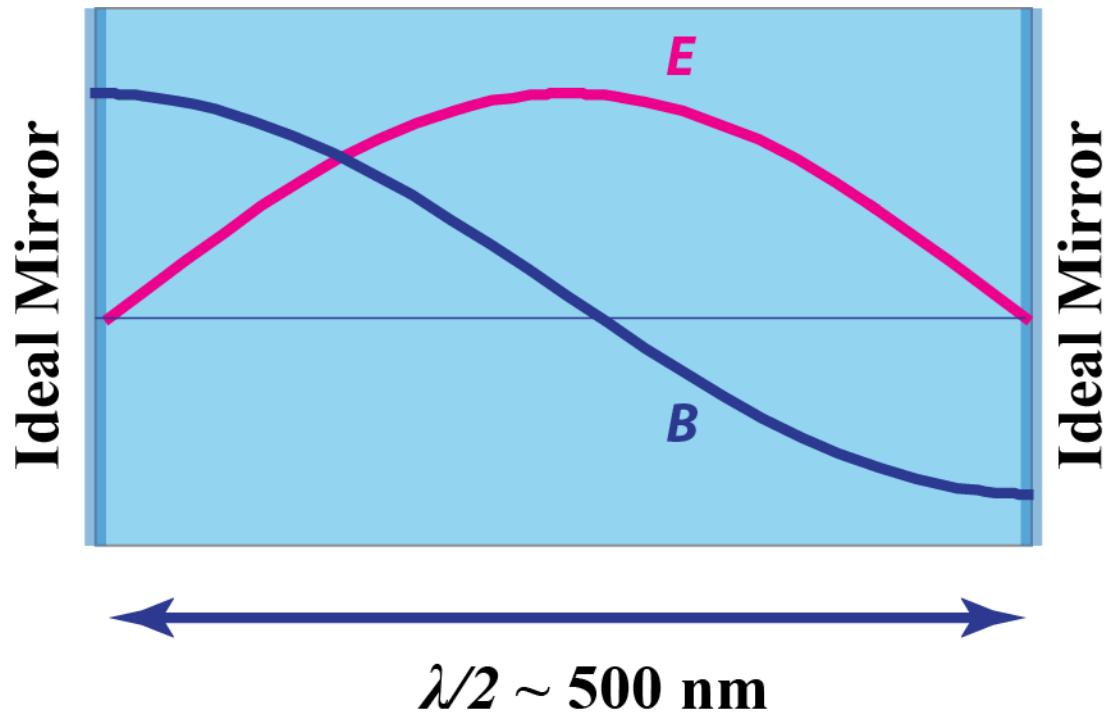
3. Adiabatic energy concentration in tapered plasmonic waveguides: theory and experiment

4. Negative refraction in nanoplasmonic waveguides (optional)

PROBLEMS IN NANOOPTICS



Concentration of optical (**electromagnetic wave**) energy: Minimum extension of electromagnetic wave in uniform space



Nanoplasmonics in a nano-nutshell

Enhanced Local Fields in Proximity of Metal Nanoparticle are Nanoscale-Localized

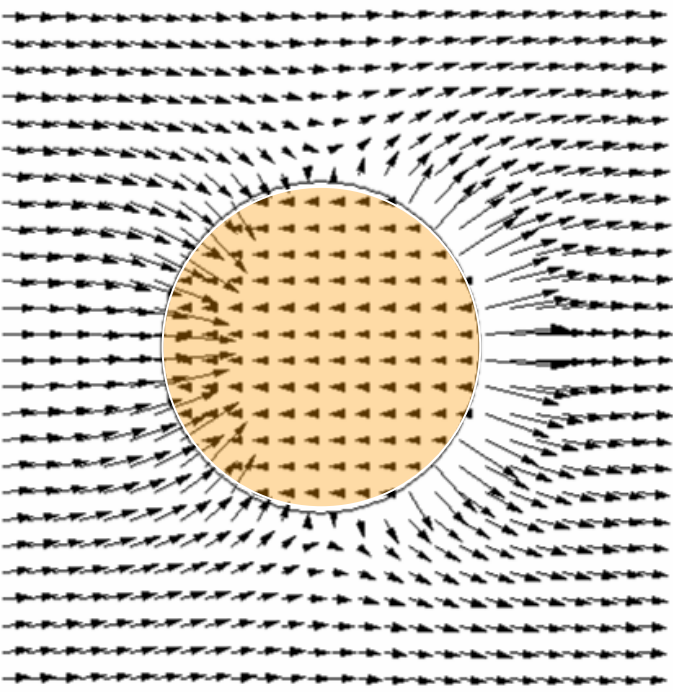
Wavelength, ~1000 nm

Mean free path, ~40 nm

Skin depth, ~25 nm

Nanoplasmonics: ~10 nm

v_F / ω Spatial dispersion/Nonlocality radius, ~1 nm



Polarizability:

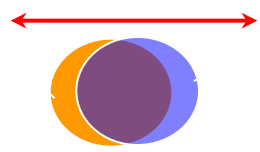
$$\alpha = R^3 \frac{\epsilon_m - \epsilon_d}{\epsilon_m + 2\epsilon_d}, \quad \epsilon_m = -2\epsilon_d$$

Field enhancement or Quality factor:

$$Q = \frac{-\text{Re } \epsilon_m}{\text{Im } \epsilon_m} \sim 10 - 100$$

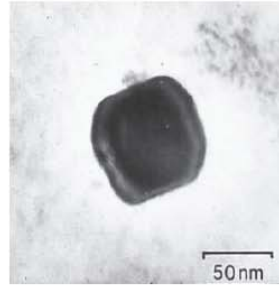
Localized Surface Plasmon:

Lattice



Electrons

Lycurgus Cup (4th Century AD): Roman Nanotechnology

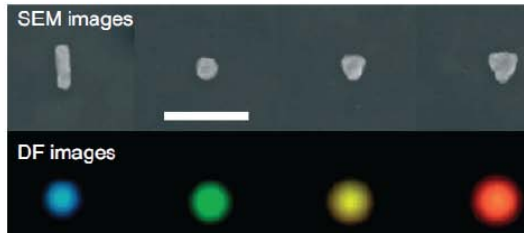
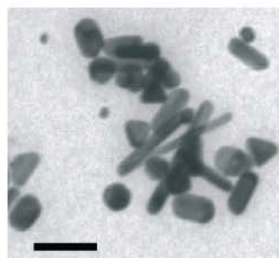
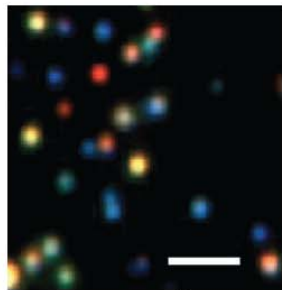


I. Freestone, N. Meeks, M. Sax, and C. Higgett, *The Lycurgus Cup - a Roman Nanotechnology*, *Gold Bull.* **40**, 270-277 (2007)

Nanoplasmonic colors are very bright. Scattering and absorption of light by them are very strong. This is due to the fact that all of the millions of electrons move in unison in plasmonic oscillations. Nanoplasmonic colors are also eternal: metal nanoparticles are stable in glass: they do not bleach and do not blink. Gold is stable under biological conditions and is not toxic *in vivo*.

© Trustees of British Museum

Colors of Silver Nanocrystals and Gold Nanoshapes



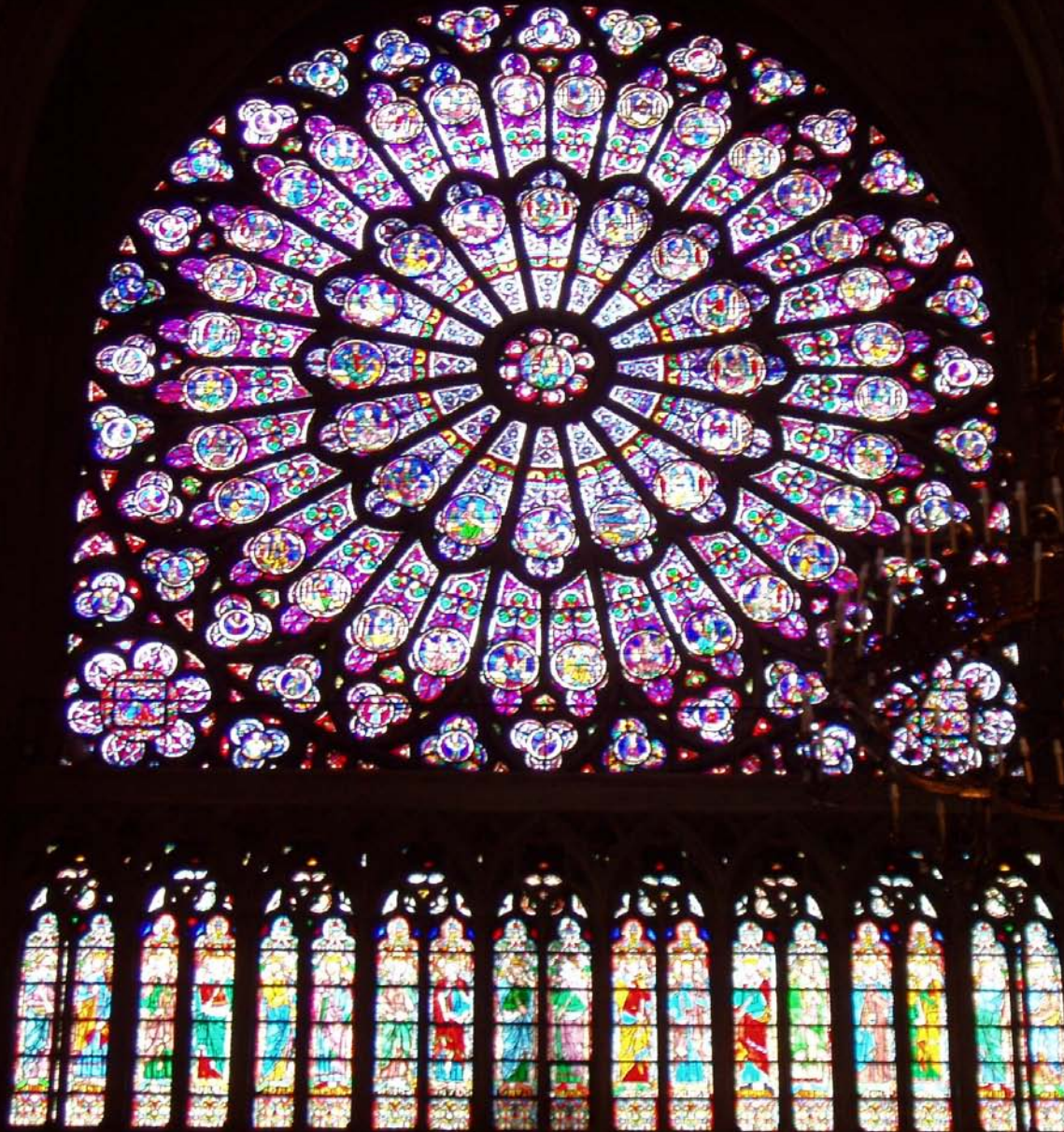
Scanning electron microscopy

Dark field optical microscopy

W. A. Murray and W. L. Barnes, *Plasmonic Materials*, *Adv. Mater.* **19**, 3771-3782 (2007) [Scale bar: 300 nm]

C. Orendorff, T. Sau, and C. Murphy, *Shape-Dependent ...*, *Small* **2**, 636-639 (2006)

Eternal nanoplasmonic colors (Notre Dame de Paris)





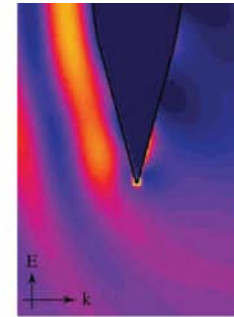
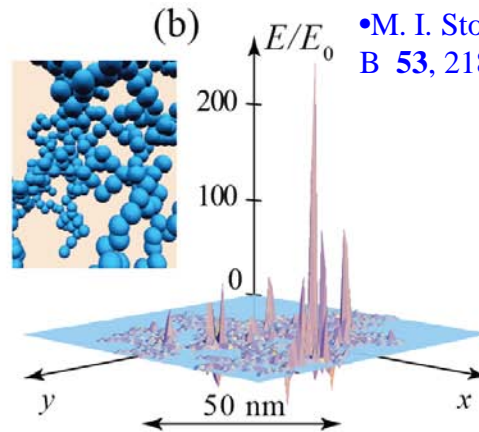
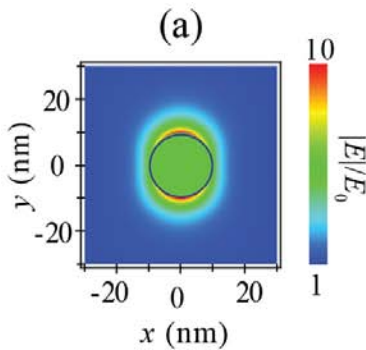
The most beautiful polychroic nanoplasmonic colors of the world: La Sainte Chapelle, Paris

Chagall Windows

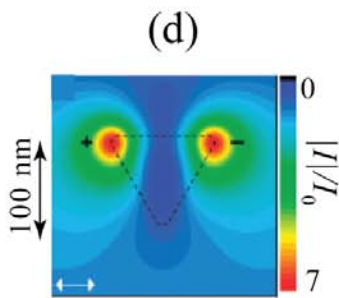
Hadassah Hospital Jerusalem



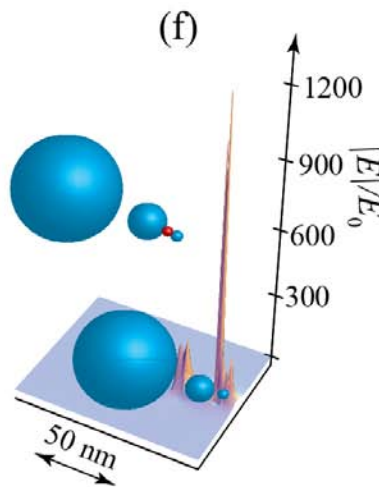
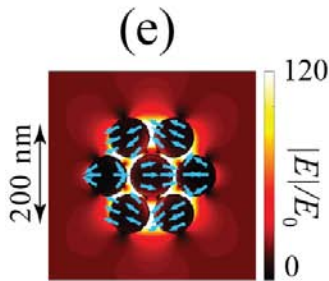
- D. P. Tsai *et al.*, *Phys. Rev. Lett.* **72**, 4149 (1994)
- M. I. Stockman *et al.*, *Phys. Rev. Lett.* **75**, 2450 (1995)
- M. I. Stockman, L. N. Pandey, and T. F. George, *Phys. Rev. B* **53**, 2183-2186 (1996)



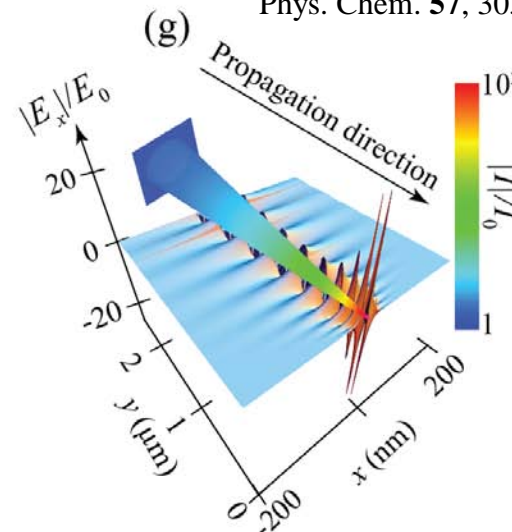
L. Novotny and S. J. Stranick, *Annual Rev. Phys. Chem.* **57**, 303-331 (2006)



M. Rang *et al.*, *Nano Lett.* **8**, 3357 (2008)



K. Li, M. I. Stockman, and D. J. Bergman, *Phys. Rev. Lett.* **91**, 227402 (2003)



M. I. Stockman, *Phys. Rev. Lett.* **93**, 137404 (2004)

- J. A. Fan *et al.*, *Science* **328**, 1135 (2010)
- M. Hentschel *et al.*, *Nano Lett.* **10**, 2721 (2010)

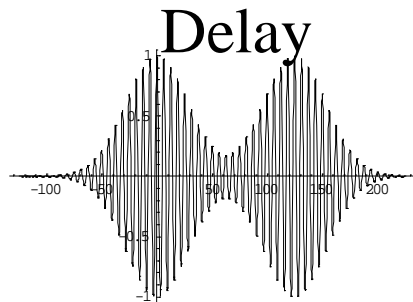
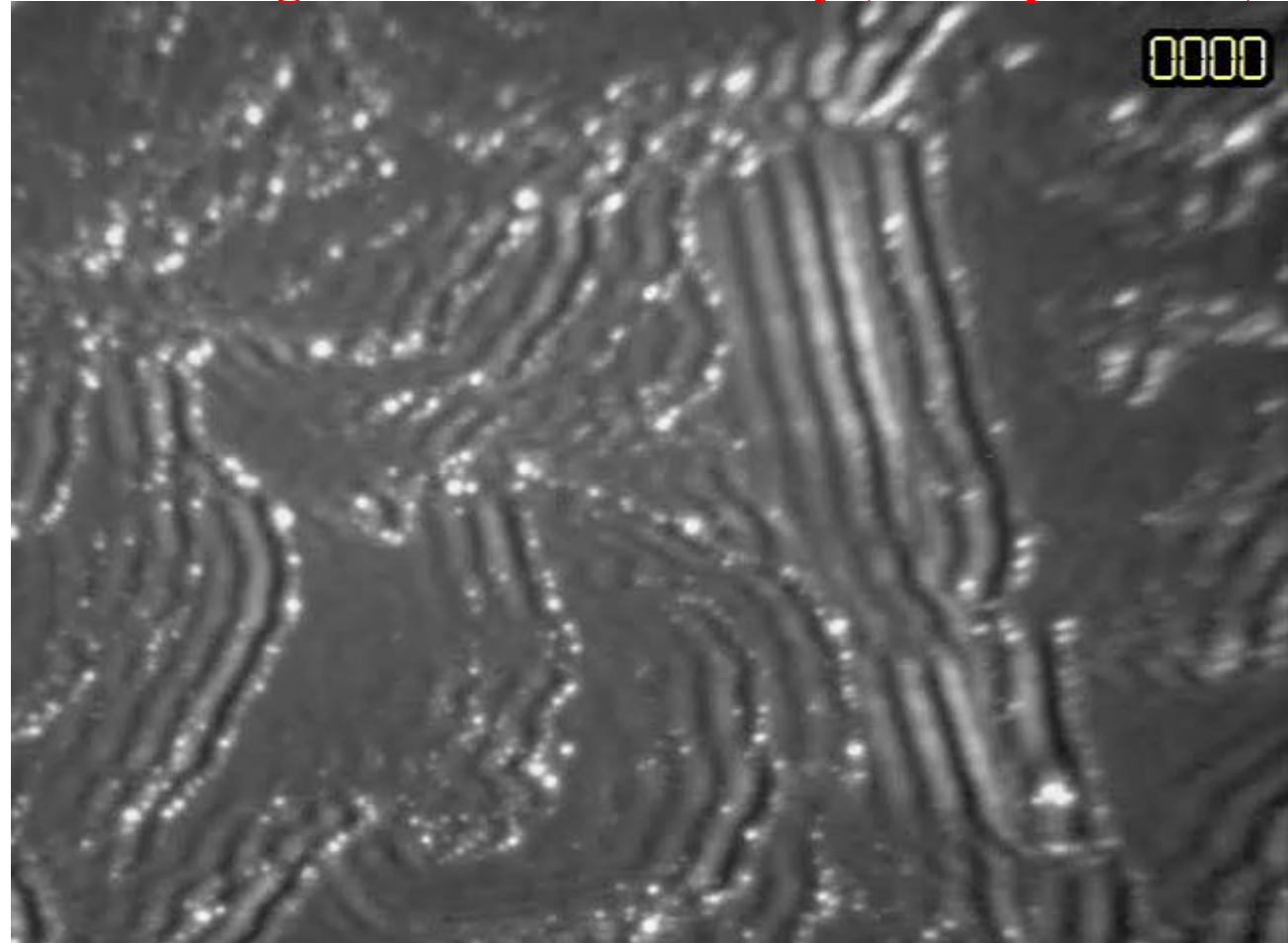
A. Kubo, K. Onda, H. Petek, Z. Sun, Y. S. Jung, and H. K. Kim, *Femtosecond Imaging of Surface Plasmon Dynamics in a Nanostructured Silver Film*, Nano Lett. 5, 1123 (2005).

PEEM Image as a Function of Delay (250 as per frame)

200 nm
↔

30 femtoseconds from life of a nanoplasmonic systems

Localized SP hot spots are deeply subwavelength as seen in PEEM (photoemission electron microscope)



Applications of Nanoplasmonics:

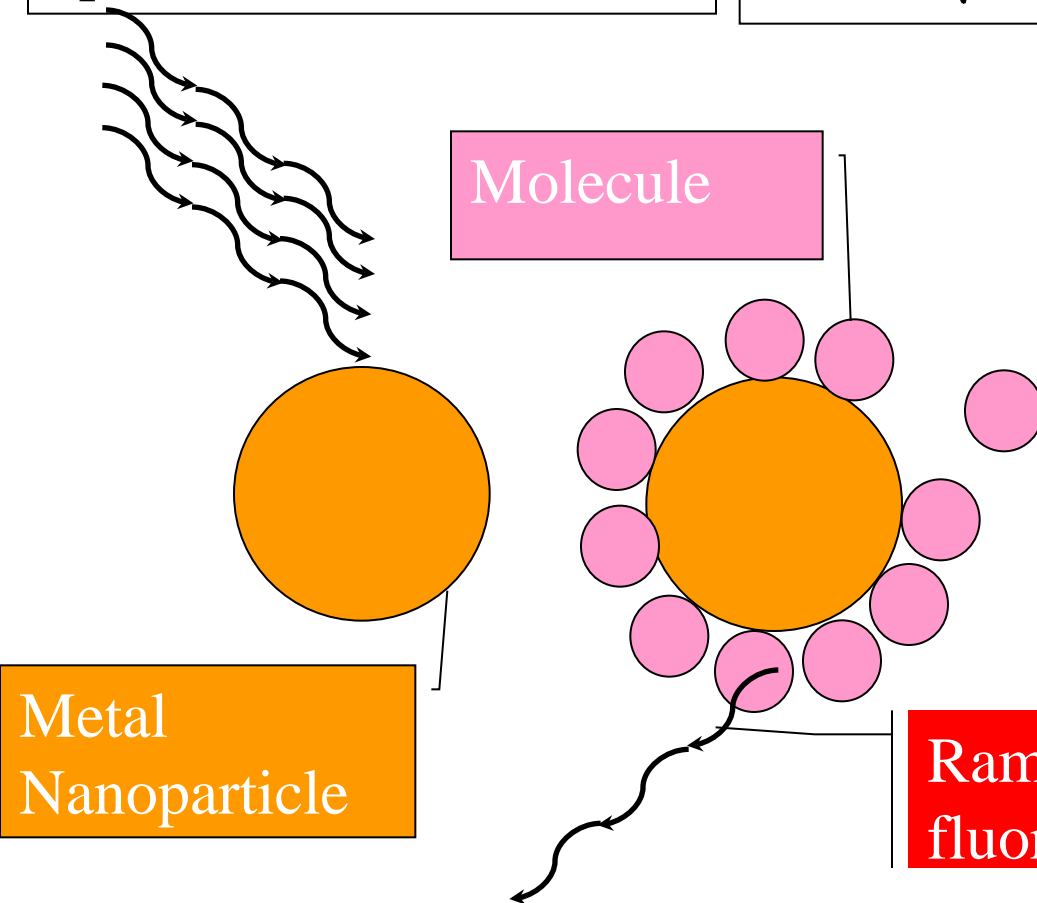
1. Ultrasensitive and express sensing and detection using both SPPs and SPs (LSPRs): see, e.g., J. N. Anker, W. P. Hall, O. Lyandres, N. C. Shah, J. Zhao, and R. P. Van Duyne, *Biosensing with Plasmonic Nanosensors*, *Nature Materials* 7, 442-453 (2008);
2. NSOM (SNOM)
3. Nanoantennas: Coupling of light to nanosystems. Extraction of light from LEDs and lasers [N. F. Yu, J. Fan, Q. J. Wang, C. Pflugl, L. Diehl, T. Edamura, M. Yamanishi, H. Kan, and F. Capasso, *Small-Divergence Semiconductor Lasers by Plasmonic Collimation*, *Nat. Phot.* 2, 564-570 (2008)]; nanostructured antennas for photodetectors and solar cells; heat-assisted magnetic memory [W. A. Challener *et al.*, *Nat. Photon.* 3, 220 (2009)]
4. Photo- and chemically stable labels and probes for biomedical research and medicine
5. Nanoplasmonic-based immunoassays and tests. Home pregnancy test (dominating the market), PSA test (clinic), troponin heart-attack test, and HIV tests (in trials)
6. Near perspective: Generation of EUV and XUV pulses
7. Thermal cancer therapy: L. R. Hirsch, R. J. Stafford, J. A. Bankson, S. R. Sershen, B. Rivera, R. E. Price, J. D. Hazle, N. J. Halas, and J. L. West, *Nanoshell-Mediated Near-Infrared Thermal Therapy of Tumors under Magnetic Resonance Guidance*, *Proc. Natl. Acad. Sci. USA* 100, 13549-13554 (2003). C. Loo, A. Lowery, N. Halas, J. West, and R. Drezek, *Immunotargeted Nanoshells for Integrated Cancer Imaging and Therapy*, *Nano Lett.* 5, 709-711 (2005)

Surface plasmon frequency shifts to red upon molecules adhesion

$$\omega_p = \frac{\omega_{0p}}{\sqrt{\epsilon_d}}$$

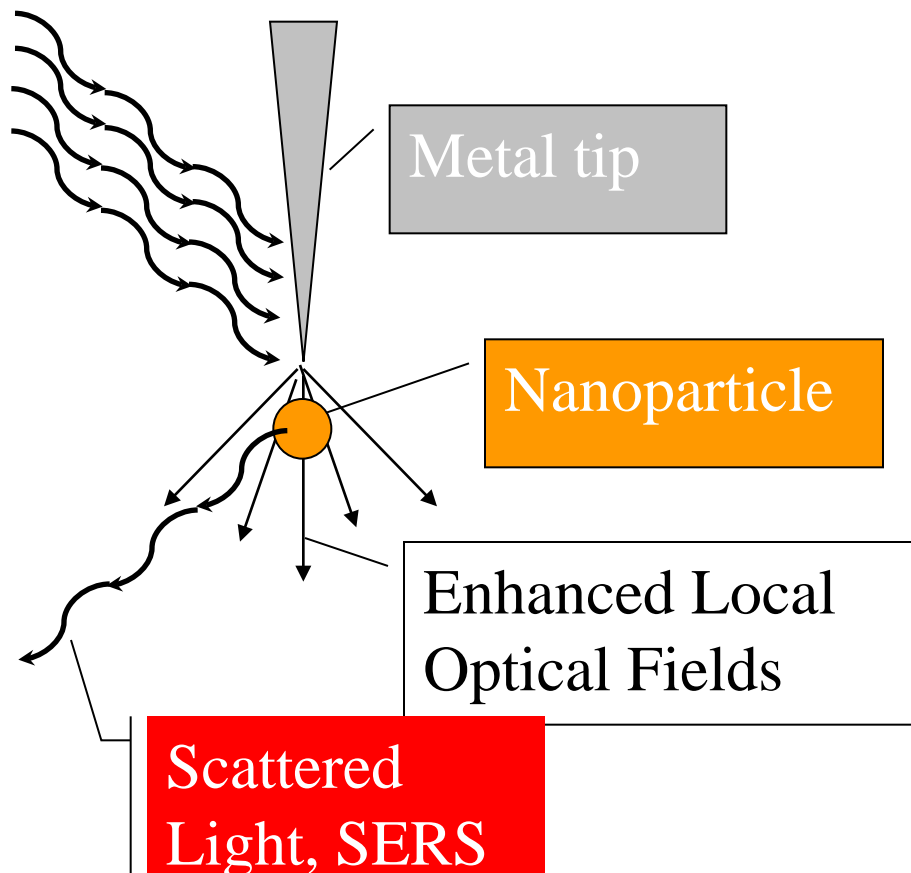
•X. Zhang, M. A. Young, O. Lyandres, and R. P. Van Duyne, *Rapid Detection of an Anthrax Biomarker by Surface-Enhanced Raman Spectroscopy*, Journal of American Chemical Society **127**, 4484 (2005).

•C. R. Yonzon, C. L. Haynes, X. Y. Zhang, J. T. Walsh, and R. P. Van Duyne, *A Glucose Biosensor Based on Surface-Enhanced Raman Scattering*, Anal. Chem. **76**, 78-85 (2004).



Raman radiation (SERS),
fluorescence, quenching, ...

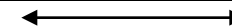
Use of Enhanced Local Fields for Nano-Microscopy



•L. Novotny and S. J. Stranick, *Near-Field Optical Microscopy and Spectroscopy with Pointed Probes*, Annual Rev. Phys. Chem. **57**, 303-331 (2006).

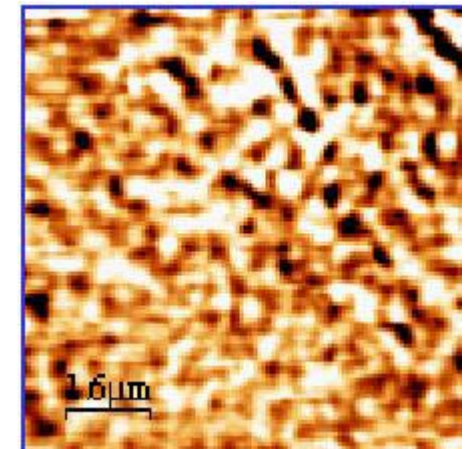
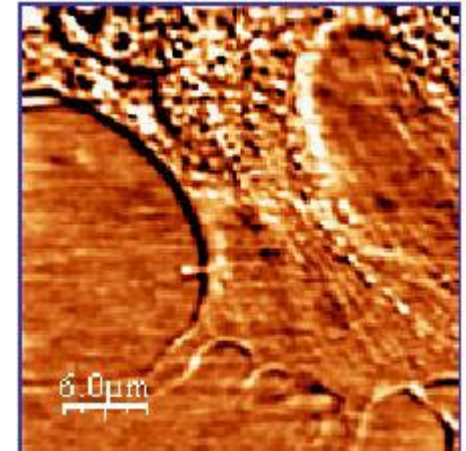
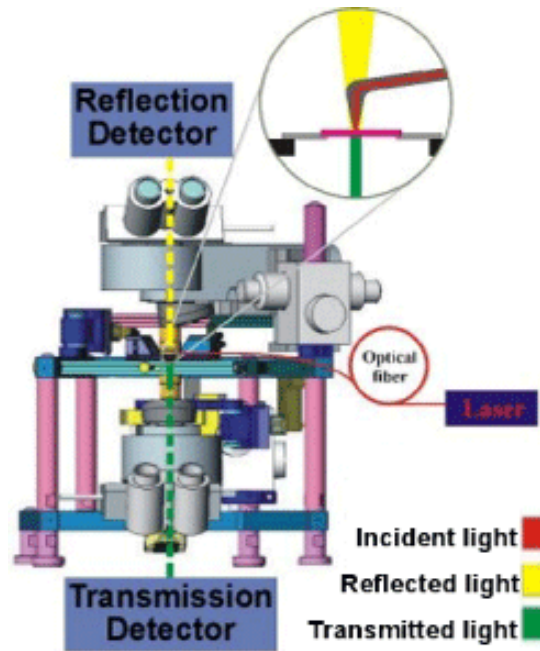
•A. Hartschuh, E. J. Sanchez, X. S. Xie, and L. Novotny, *High-Resolution Near-Field Raman Microscopy of Single-Walled Carbon Nanotubes*, Phys. Rev. Lett. **90**, 095503 -1-4 (2003).

Nanoscale





NSOM images of healthy human dermal fibroblasts in liquid obtained in transmission mode with a Nanonics cantilevered tip with a gold nanosphere





Contents lists available at ScienceDirect

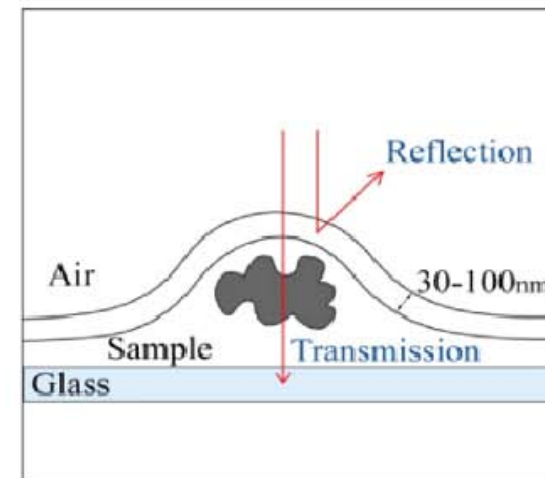
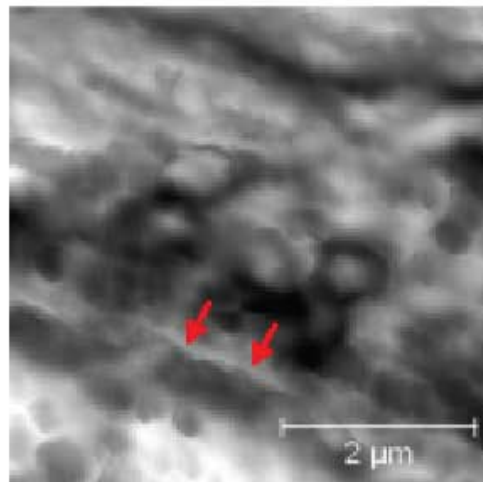
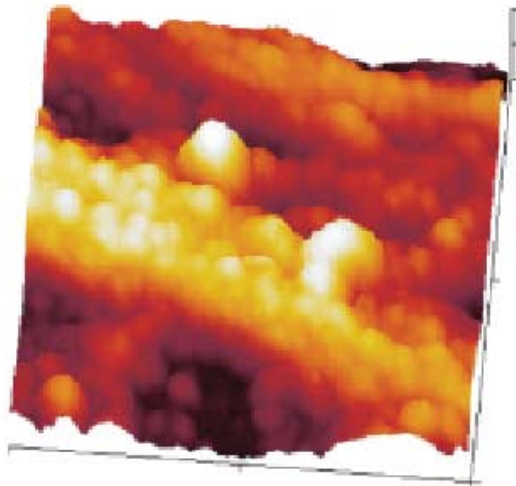
NeuroImage

journal homepage: www.elsevier.com/locate/ynimg



Novel approaches for scanning near-field optical microscopy imaging of oligodendrocytes in culture

E. Trevisan^a, E. Fabbretti^{b,c}, N. Medic^d, B. Troian^e, S. Prato^e, F. Vita^f, G. Zabucchi^d, M. Zweyer^{a,*}



Chirality Changes in Carbon Nanotubes Studied with Near-Field Raman Spectroscopy

Neil Anderson, Achim Hartschuh, and Lukas Novotny

Nano Lett. 577 – 582 (2007); DOI: [10.1021/nl0622496](https://doi.org/10.1021/nl0622496)

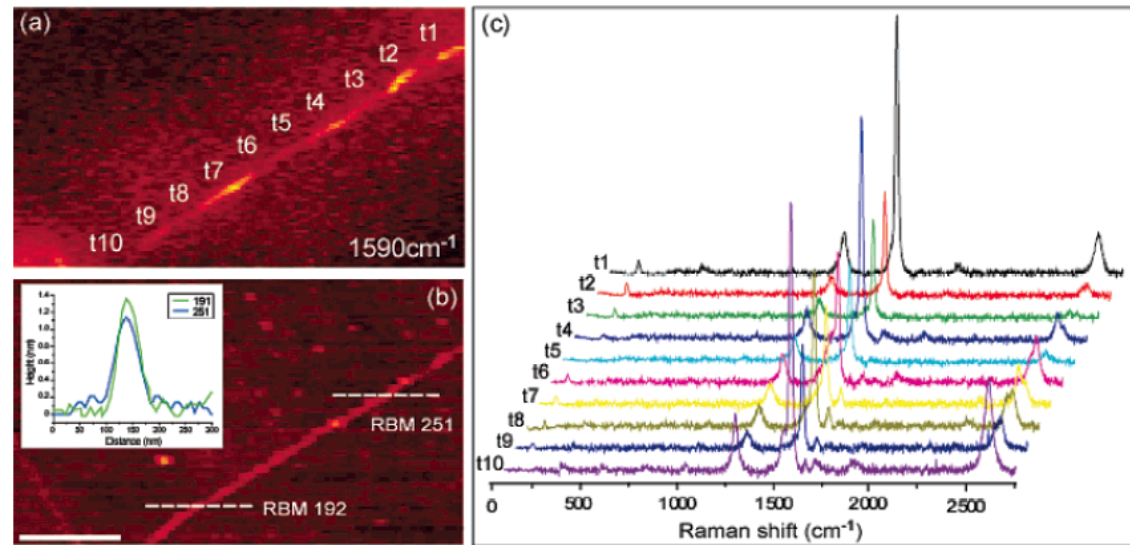


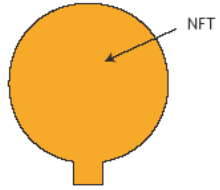
Figure 1. Near-field Raman imaging and spectroscopy: near-field Raman image (a) and corresponding topography image (b) of an isolated SWNT, where the optical resolution was determined to be 40 nm (fwhm). Also shown are a series of tip-enhanced Raman spectra (c) acquired along the length of the SWNT. From the recorded spectra, two resonant RBM phonons are detected. One RBM phonon frequency is detected at 251 cm^{-1} , from which we assign a semiconducting chirality. The second RBM phonon frequency recorded from the lower section of the SWNT is centered at 192 cm^{-1} , from which we assign a metallic chirality. See main text for details. The inset of (b) displays two cross-sectional profiles acquired from both the upper and lower sections, respectively, revealing that the expected diameter change occurs as the SWNT undergoes the transition from a semiconducting to metallic chirality. Scale bar denotes 200 nm and is valid for both (a) and (b).

Next generation of scanning
near-field optical microscopy
(SNOM) with chemical
mapping:

Adiabatic concentration of
optical energy and giant
surface-enhanced Raman
scattering (SERS); resolution 7
nm.s

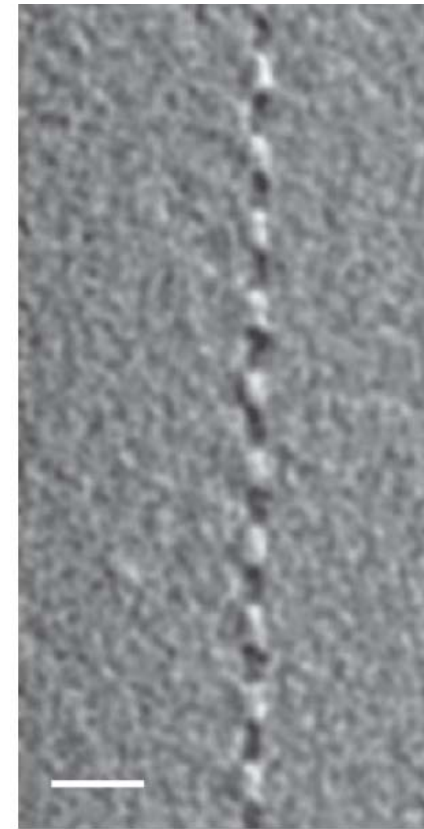
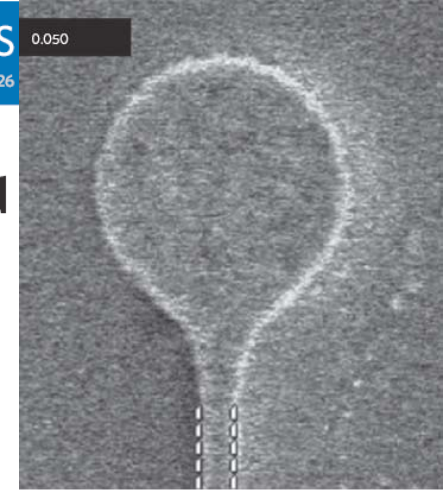
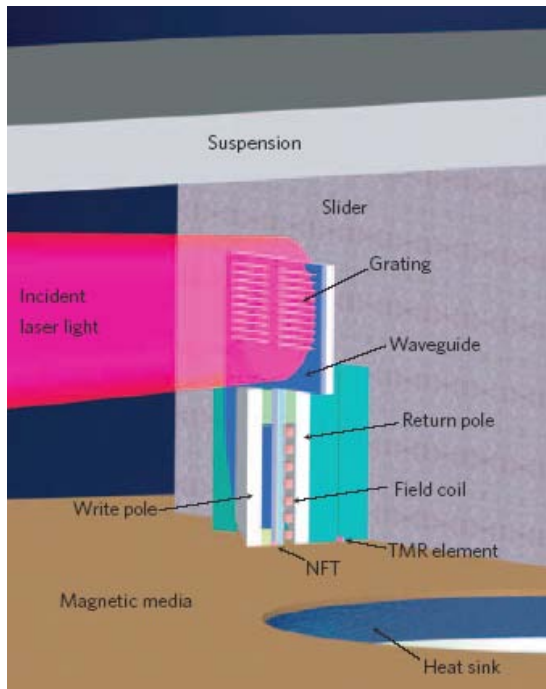
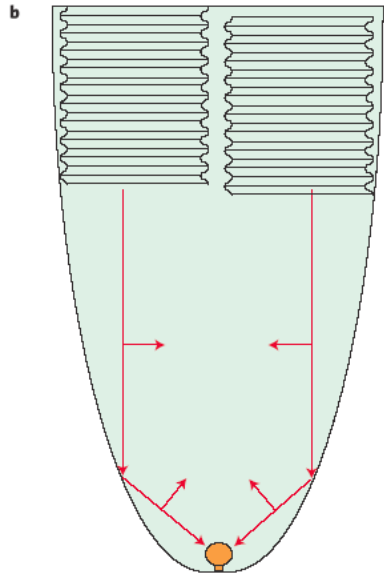
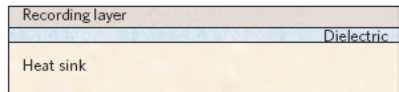
(to be discussed in the course)



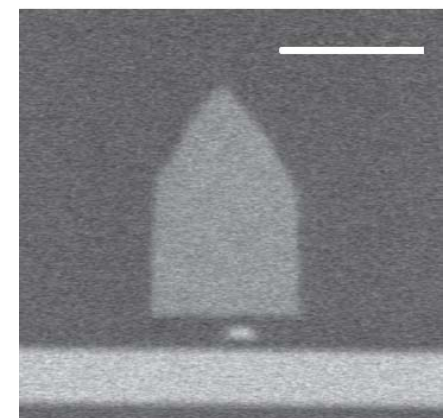


Heat-assisted magnetic recording by a near-field transducer with efficient optical energy transfer

W. A. Challener*, Chubing Peng, A. V. Itagi, D. Karns, Wei Peng, Yingguo Peng, XiaoMin Yang, Xiaobin Zhu, N. J. Gokemeijer, Y.-T. Hsia, G. Ju, Robert E. Rottmayer, Michael A. Seigler and E. C. Gage



MFM image of a recorded track. The track width is ~ 70 300 nm.



Nanometre-scale germanium photodetector enhanced by a near-infrared dipole antenna

LIANG TANG^{1*}, SUKRU EKIN KOCABAS¹, SALMAN LATIF¹, ALI K. OKYAY², DANY-SEBASTIEN LY-GAGNON¹, KRISHNA C. SARASWAT² AND DAVID A. B. MILLER¹

¹Ginzton Laboratory, Stanford University, Stanford, California 94305, USA

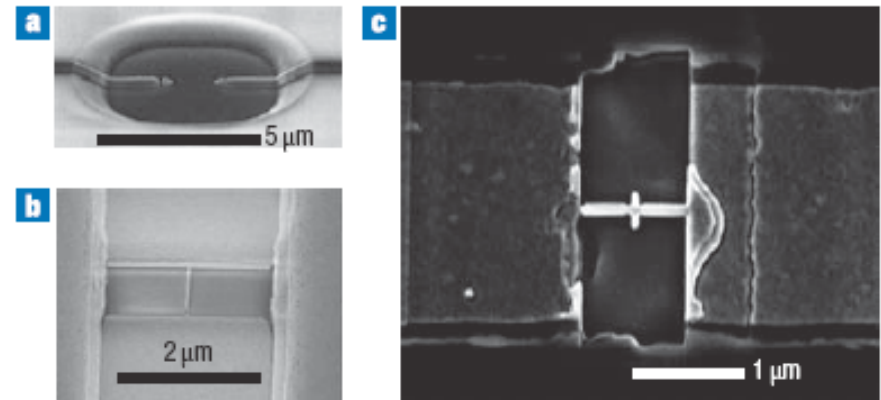
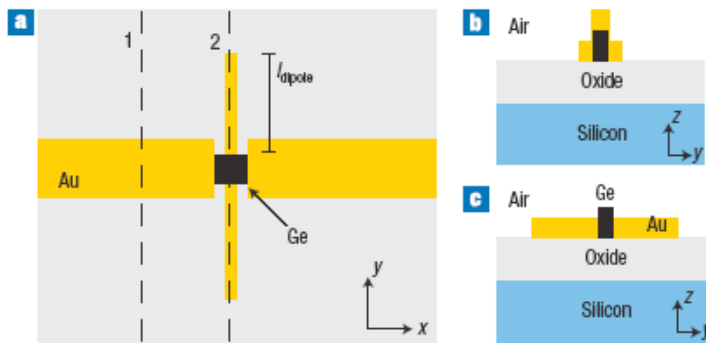


Figure 3 Scanning electron microscopy (SEM) images of the fabricated devices. **a**, Silicon seeding window with 2- μm -wide germanium crystalline lines. **b**, 60-nm-wide and 2- μm -long germanium nanowire fabricated by the first FIB step. **c**, An open-sleeve dipole antenna detector with $l_{\text{dipole}} = 155 \text{ nm}$ (this image is rotated by 90° in relation to that in **b**). (Charging due to a thick oxide layer limits the resolution in this SEM image.)

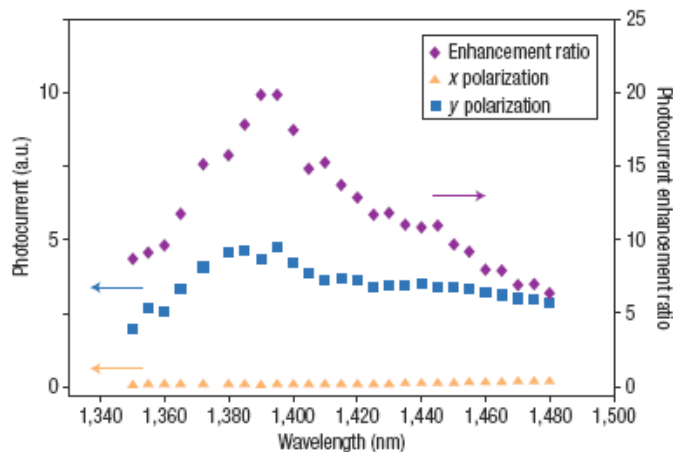
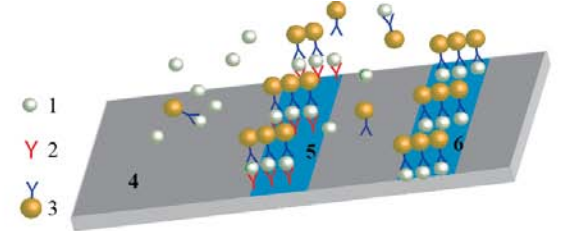
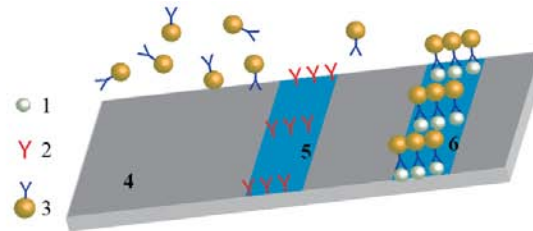


Figure 5 Measured photocurrent responses for light polarization in the y and x directions. The wavelengths were 1,350–1,480 nm for the detector with $l_{\text{dipole}} = 160 \text{ nm}$.

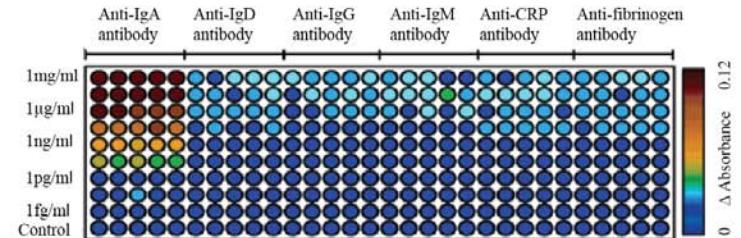
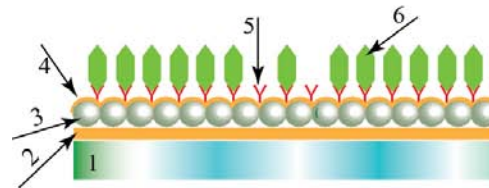
SP Sensing and Detection



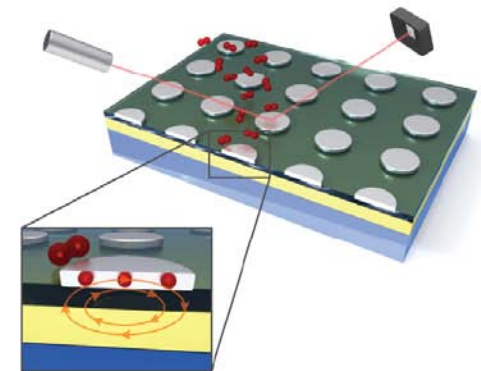
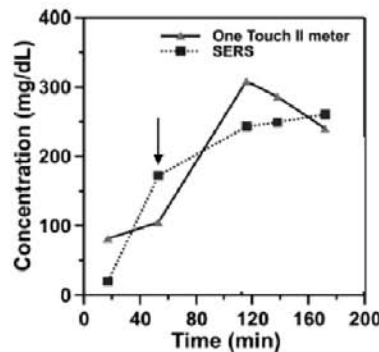
- 1 – Antigen (hCG)
- 2 – Primary antibody
- 3 – Gold nanosphere functionalized with secondary antibody



- 1 – Substrate
- 2 – Gold nanofilm
- 3 – Latex nanospheres
- 4 – Gold nanolayer
- 5 – Antibodies
- 6 - Analyte molecules



Adapted from:
T. Endo et al., *Anal. Chem.* **78**, 6465 (2006).

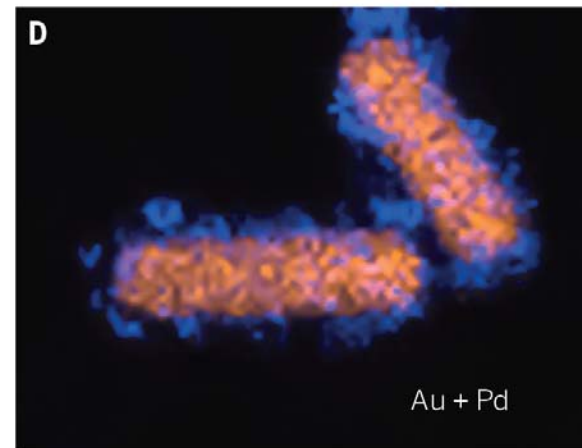
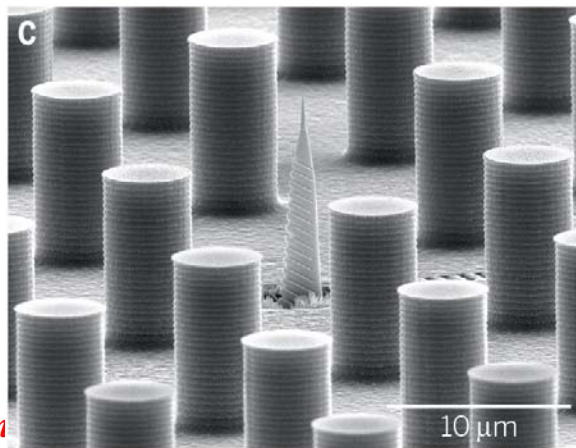
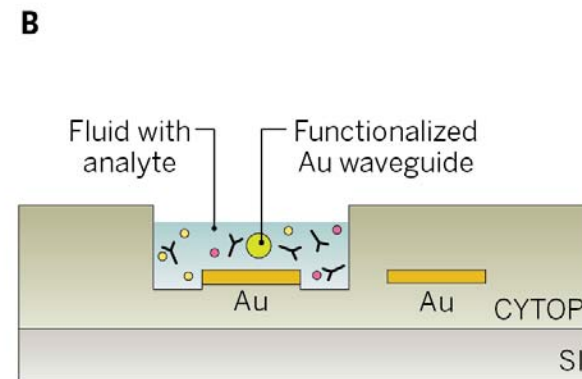
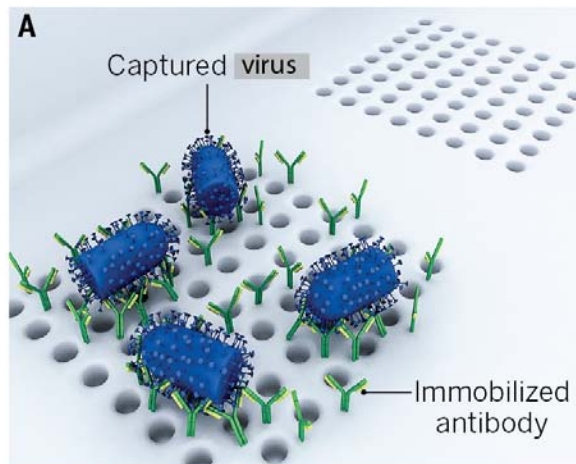


J.N. Anker et al., *Nature Materials* **7**, 442 (2008)

N. Liu et al., *Nat. Mater.* **advance online publication DOI: 10.1038/nmat3029 (2011)**

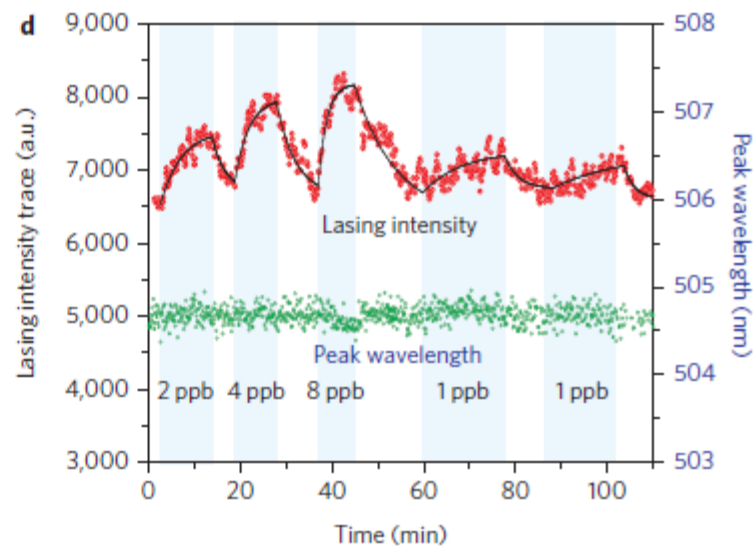
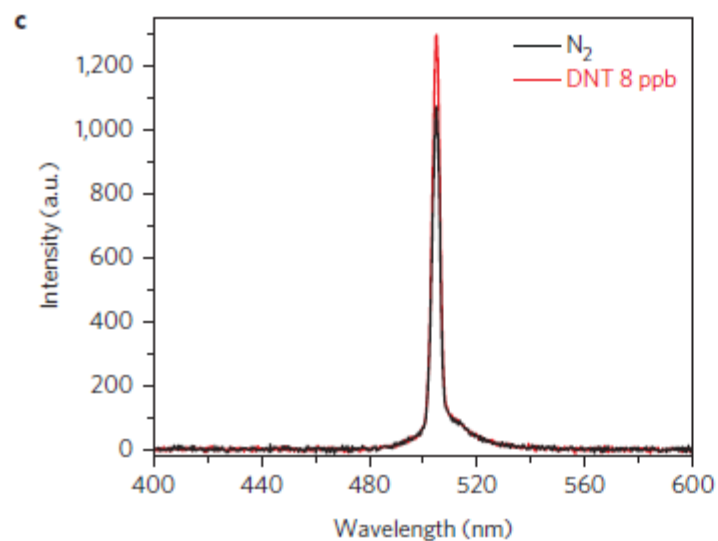
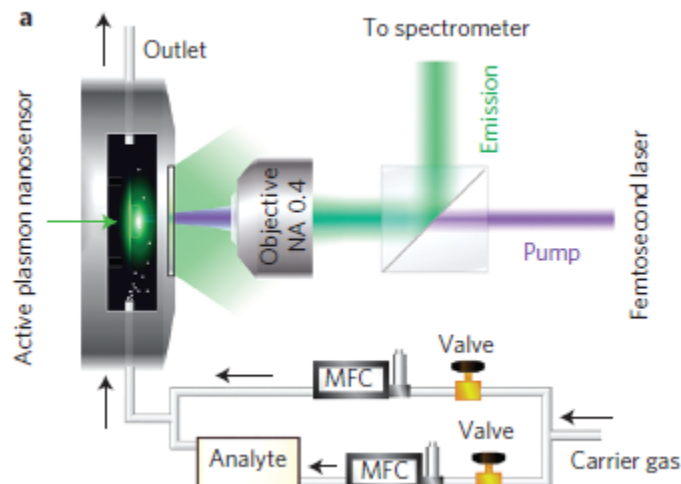
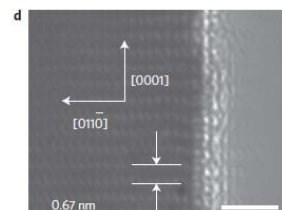
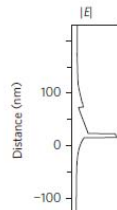
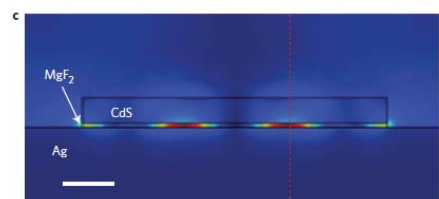
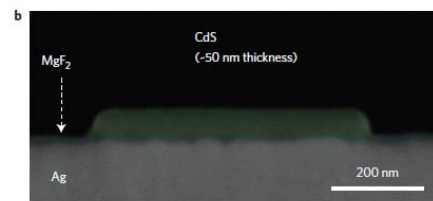
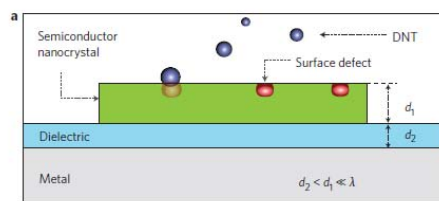
M. I. Stockman, *Nanoplasmonic Sensing and Detection*, Science **348**, 287-288 (2015).

Capture and detection



Explosives detection in a lasing plasmon nanocavity

Ren-Min Ma[†], Sadao Ota[†], Yimin Li¹, Sui Yang¹ and Xiang Zhang^{1,2*}

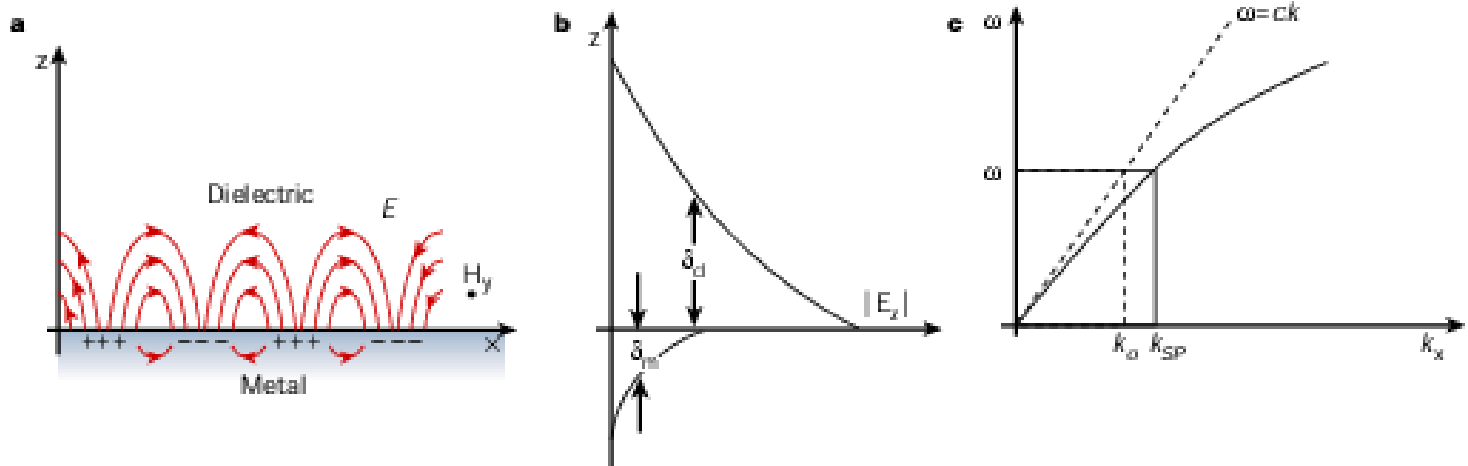


insight review articles

William L. Barnes, Alain Dereux & Thomas W. Ebbesen, Nature 424, 824 (2003)

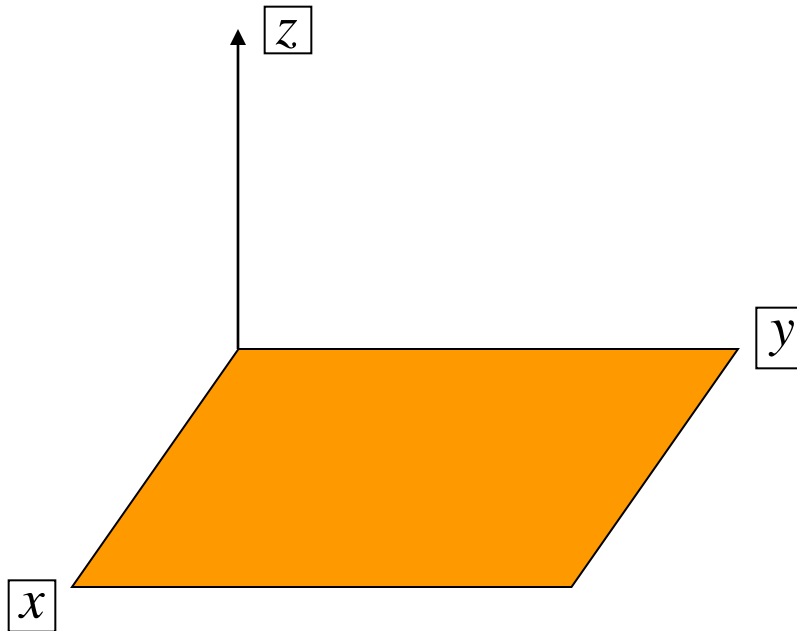
Box 1
Surface plasmon basics

SPs at the interface between a metal and a dielectric material have a combined electromagnetic wave and surface charge character as shown in **a**. They are transverse magnetic in character (\mathbf{H} is in the y direction), and the generation of surface charge requires an electric field normal to the surface. This combined character also leads to the field component perpendicular to the surface being enhanced near the surface and decaying exponentially with distance away from it (**b**). The field in this perpendicular direction is said to be evanescent, reflecting the bound, non-radiative nature of SPs, and prevents power from propagating away from the surface. In the dielectric medium above the metal, typically air or glass, the decay length of the field, δ_d , is of the order of half the wavelength of light involved, whereas the decay length into the metal, δ_m , is determined by the skin depth. **c**, The dispersion curve for a SP mode shows the momentum mismatch problem that must be overcome in order to couple light and SP modes together, with the SP mode always lying beyond the light line, that is, it has greater momentum ($\hbar k_{SP}$) than a free space photon ($\hbar k_0$) of the same frequency ω .



SURFACE PLASMON POLARITONS

Assume that we have a plane interface and consider propagation in the xy plane.



Maxwell Equations in the absence of the external currents and charges:

for $\mathbf{E}, \mathbf{H} \propto \exp(-i\omega t)$

$$\nabla \times \mathbf{E} = -\frac{1}{c} \frac{\partial \mathbf{B}}{\partial t} \quad \Rightarrow \quad \nabla \times \mathbf{E} = ik_0 \mu \mathbf{H}$$

$$\nabla \times \mathbf{H} = \frac{1}{c} \frac{\partial \mathbf{D}}{\partial t} \quad \Rightarrow \quad \nabla \times \mathbf{H} = -ik_0 \epsilon \mathbf{E}, \quad \text{where } k_0 \equiv \frac{\omega}{c}$$

$$\nabla \mathbf{D} = 0,$$

$$\nabla \mathbf{H} = 0; \quad \mathbf{F} = e\mathbf{E} + \frac{e}{c} [\mathbf{v} \times \mathbf{B}] \quad \text{Lorentz formula}$$

See, e.g., L. D. Landau and E. M. Lifshitz, *Electrodynamics of Continuous Media* (Pergamon, Oxford and New York, 1984).

General type
of linear
response

$$\mathbf{D}(\mathbf{r}, t) = \int_{-\infty}^{\infty} \boldsymbol{\varepsilon}(\mathbf{r} - \mathbf{r}', t - t') \mathbf{E}(\mathbf{r}', t') dt' d^3 r'$$

$$\mathbf{B}(\mathbf{r}, t) = \int_{-\infty}^{\infty} \boldsymbol{\mu}(\mathbf{r} - \mathbf{r}', t - t') \mathbf{H}(\mathbf{r}', t') dt' d^3 r'$$

Local
response

$$\mathbf{D}(\mathbf{r}, t) = \int_{-\infty}^{\infty} \boldsymbol{\varepsilon}(\mathbf{r}, t - t') \mathbf{E}(\mathbf{r}, t') dt' \Rightarrow \mathbf{D}(\omega) = \boldsymbol{\varepsilon}(\omega) \mathbf{E}(\omega)$$

$$\mathbf{B}(\mathbf{r}, t) = \int_{-\infty}^{\infty} \boldsymbol{\mu}(\mathbf{r}, t - t') \mathbf{H}(\mathbf{r}, t') dt' \Rightarrow \mathbf{B}(\omega) = \boldsymbol{\mu}(\omega) \mathbf{H}(\omega)$$

$$\mathbf{D}(\omega) = \int_{-\infty}^{\infty} \mathbf{D}(t) e^{i\omega t} dt, \quad \mathbf{D}(t) = \int_{-\infty}^{\infty} \mathbf{D}(\omega) e^{-i\omega t} \frac{d\omega}{2\pi},$$

Relation between permittivity and conductivity (Optional)

$$\text{Continuity eq. : } \frac{\partial \rho(t)}{\partial t} + \frac{\partial \mathbf{j}(t)}{\partial \mathbf{r}} = 0 \quad \Rightarrow$$

$$\rho = -\frac{\partial \mathbf{P}}{\partial \mathbf{r}} \quad \Rightarrow \quad \mathbf{j}(t) = \frac{\partial \mathbf{P}(t)}{\partial t} \quad \Rightarrow \quad \mathbf{j}(\omega) = -i\omega \mathbf{P}(\omega)$$

$$\mathbf{D}(\omega) = \mathbf{E}(\omega) + 4\pi \mathbf{P}(\omega) = \varepsilon(\omega) \mathbf{E}(\omega) \quad \Rightarrow \quad \mathbf{P}(\omega) = \frac{\varepsilon(\omega) - 1}{4\pi} \mathbf{E}(\omega)$$

$$\mathbf{j}(\omega) = -i\omega \frac{\varepsilon(\omega) - 1}{4\pi} \mathbf{E}(\omega)$$

$$\mathbf{j}(\omega) = \sigma(\omega) \mathbf{E}(\omega) \quad \Rightarrow \quad \begin{cases} \sigma(\omega) = -i\omega \frac{\varepsilon(\omega) - 1}{4\pi} \\ \varepsilon(\omega) = 1 + i \frac{4\pi}{\omega} \sigma(\omega) \end{cases}$$

Seeking for solution as a TM wave

$$\mathbf{H} = (H_x(y, z, t), 0, 0)$$

(To be confirmed by equations)

$$\mathbf{E} = (0, E_y(y, z, t), E_z(y, z, t))$$

Spatio-temporal dependence:

$$H_x(y, z, t) = H_x(z) \exp(iky - i\omega t)$$

$$E_i(y, z, t) = E_i(z) \exp(iky - i\omega t), \quad i = y, z$$

Wave equations are obtained by applying curl operation to Maxwell equations:

$$(\nabla^2 + k_0^2 \epsilon \mu) \mathbf{H} = 0 \quad \Rightarrow \quad \left(\frac{\partial^2}{\partial z^2} - k^2 + k_0^2 \epsilon \mu \right) H_x = 0$$

$$(\nabla^2 + k_0^2 \epsilon \mu) \mathbf{E} = 0 \quad \Rightarrow \quad \left(\frac{\partial^2}{\partial z^2} - k^2 + k_0^2 \epsilon \mu \right) E_{y,z} = 0$$

Seeking

$$H_x(z) \propto \exp(\pm \kappa z), \quad E_{y,z}(z) \propto \exp(\pm \kappa z)$$

From the wave equations: $k_0^2 \epsilon \mu = k^2 - \kappa^2$, $k_0 = \frac{\omega}{c}$;

$$\nabla \times \mathbf{H} = -ik_0 \epsilon \mathbf{E} \Rightarrow$$

$$x: \quad \frac{\partial H_z}{\partial y} - \frac{\partial H_y}{\partial z} = -ik_0 \epsilon E_x \Rightarrow E_x = 0$$

$$y: \quad \frac{\partial H_x}{\partial z} - \frac{\partial H_z}{\partial x} = -ik_0 \epsilon E_y \Rightarrow E_y = \pm \frac{i\kappa}{k_0 \epsilon} H_x$$

$$z: \quad \frac{\partial H_y}{\partial x} - \frac{\partial H_x}{\partial y} = -ik_0 \epsilon E_z \Rightarrow E_z = \frac{k}{k_0 \epsilon} H_x$$

Because we have already satisfied the wave equations, the second Maxwell equation is satisfied identically

Boundary conditions are continuity across the interface plane of

$$H_x \quad \text{and} \quad E_y = \frac{i}{k_0 \epsilon} \frac{\partial H_x}{\partial z}$$

For a planar layered medium, surface plasmon polariton (SPP) is a TM wave where in an i -th medium layer at a point (y, z) for a wave propagating in the y direction

$$H_x(i, y, z) = [A_i \exp(\kappa_i z) + B_i \exp(-\kappa_i z)] \exp(iky),$$

$$E_y(i, y, z) = \frac{i\kappa_i}{\epsilon_i k_0} [A_i \exp(\kappa_i z) - B_i \exp(-\kappa_i z)] \exp(iky),$$

$$E_z(i, y, z) = \frac{k}{\epsilon_i} H_x(i, y, z);$$

$$k \equiv k_y; \quad k_0^2 \epsilon \mu = k^2 - \kappa^2, \quad k_0 = \frac{\omega}{c}; \quad i = 1, 2, \dots \text{ is layer number}$$

For metal/dielectric interface

Boundary conditions :

$$H_x(1, y, z) = H_x(2, y, z)$$

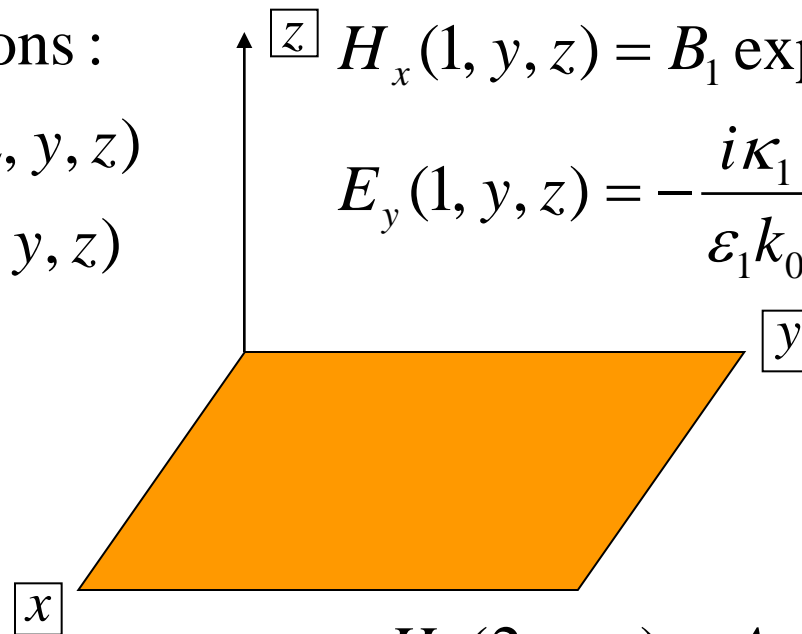
$$E_y(1, y, z) = E_y(2, y, z)$$

These conditions

reduce to :

$$B_1 = A_2$$

$$\frac{\kappa_1}{\epsilon_1} = -\frac{\kappa_2}{\epsilon_2}$$



$$H_x(1, y, z) = B_1 \exp(-\kappa_1 z) \exp(iky),$$

$$E_y(1, y, z) = -\frac{i\kappa_1}{\epsilon_1 k_0} B_1 \exp(-\kappa_1 z) \exp(iky),$$

$$H_x(2, y, z) = A_2 \exp(\kappa_2 z) \exp(iky),$$

$$E_y(2, y, z) = \frac{i\kappa_2}{\epsilon_2 k_0} A_2 \exp(\kappa_2 z) \exp(iky).$$

Boundary conditions :

$$\frac{\kappa_1}{\varepsilon_1} = -\frac{\kappa_2}{\varepsilon_2}$$

Wave equations :

$$k_0^2 \varepsilon_1 = k^2 - \kappa_1^2$$

$$k_0^2 \varepsilon_2 = k^2 - \kappa_2^2$$

Definition :

$$k_0 = \frac{\omega}{c}$$

Transforming :

$$\frac{\kappa_1^2}{\varepsilon_1^2} = \frac{\kappa_2^2}{\varepsilon_2^2} \Rightarrow$$

Substituting : \Downarrow

$$\frac{k_0^2 \varepsilon_1 - k^2}{\varepsilon_1^2} = \frac{k_0^2 \varepsilon_2 - k^2}{\varepsilon_2^2}$$

Algebraically solving for k^2 : $k^2 = k_0^2 \frac{\varepsilon_1 \varepsilon_2}{\varepsilon_1 + \varepsilon_2}$

Finding by substitution : $\kappa_1^2 = -k_0^2 \frac{\varepsilon_1^2}{\varepsilon_1 + \varepsilon_2}$, $\kappa_2^2 = -k_0^2 \frac{\varepsilon_2^2}{\varepsilon_1 + \varepsilon_2}$.

Metal-Dielectric Interface

For a two-medium system, the SPP wave vector is found as a function of frequency (dispersion relation):

$$k = \frac{\omega}{c} \sqrt{\frac{\epsilon_1 \epsilon_2}{\epsilon_1 + \epsilon_2}}$$

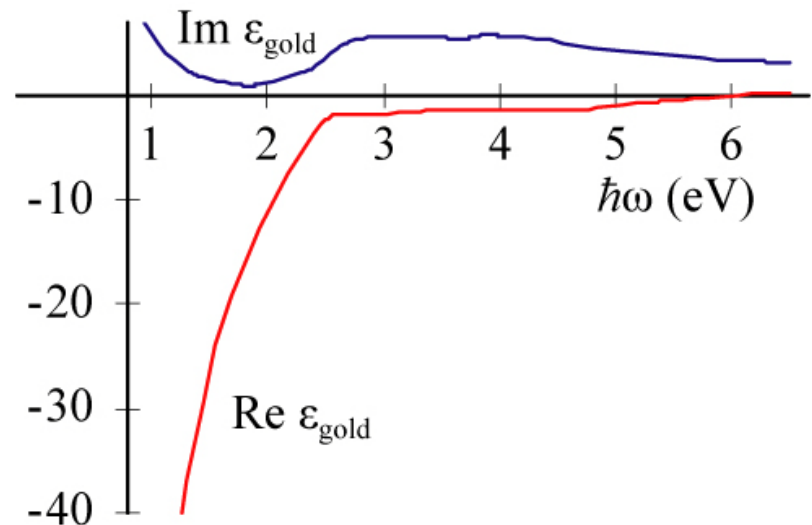
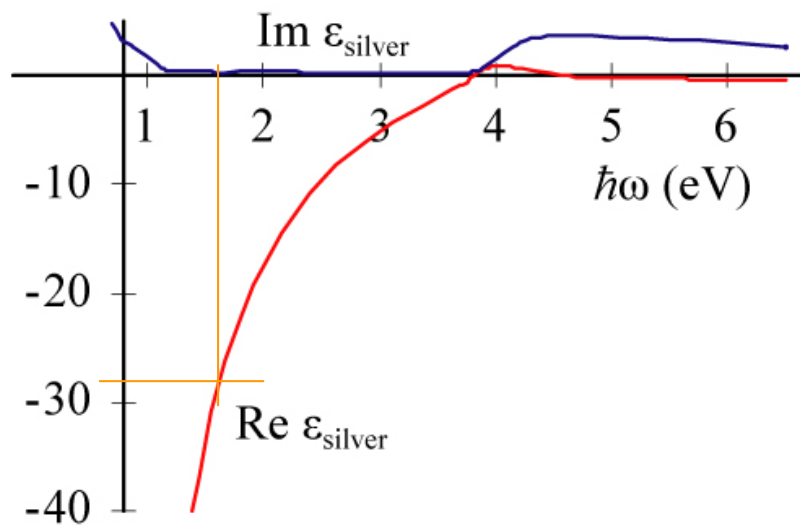
Evanescent decay exponents in these two media are found as

$$K_1 = \frac{\omega}{c} \sqrt{-\frac{\epsilon_1^2}{\epsilon_1 + \epsilon_2}} \quad K_2 = \frac{\omega}{c} \sqrt{-\frac{\epsilon_2^2}{\epsilon_1 + \epsilon_2}}$$

From these, it follows that for the existence of SPPs, it is necessary and sufficient that $\epsilon_1 + \epsilon_2 < 0$ and $\epsilon_1 \epsilon_2 < 0$

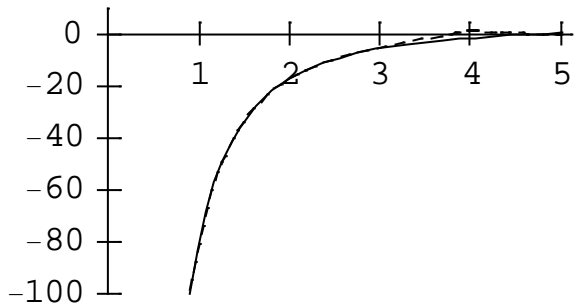
Dielectric permittivity for silver and gold in optical region

P. B. Johnson and R. W. Christy, "Optical-Constants of Noble-Metals," *Physical Review B* **6**, 4370-4379 (1972).



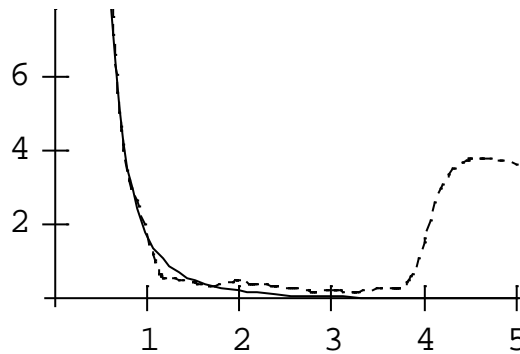
$$\lambda[\mu] = \frac{1.24}{\omega[\text{eV}]}$$

Drude formula:
$$\epsilon = \epsilon_0 - \frac{\omega_p^2}{\omega(\omega + i\gamma)}$$



Re ϵ ; $\epsilon_0 = 3.6$; $\omega_p = 9.1$ eV

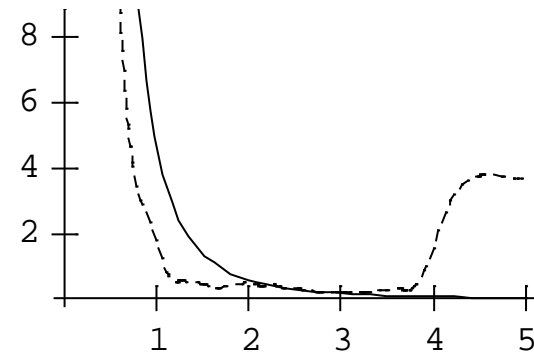
Im ϵ ; $\gamma = 0.02$ eV



ω (eV)

Fit to near-ir

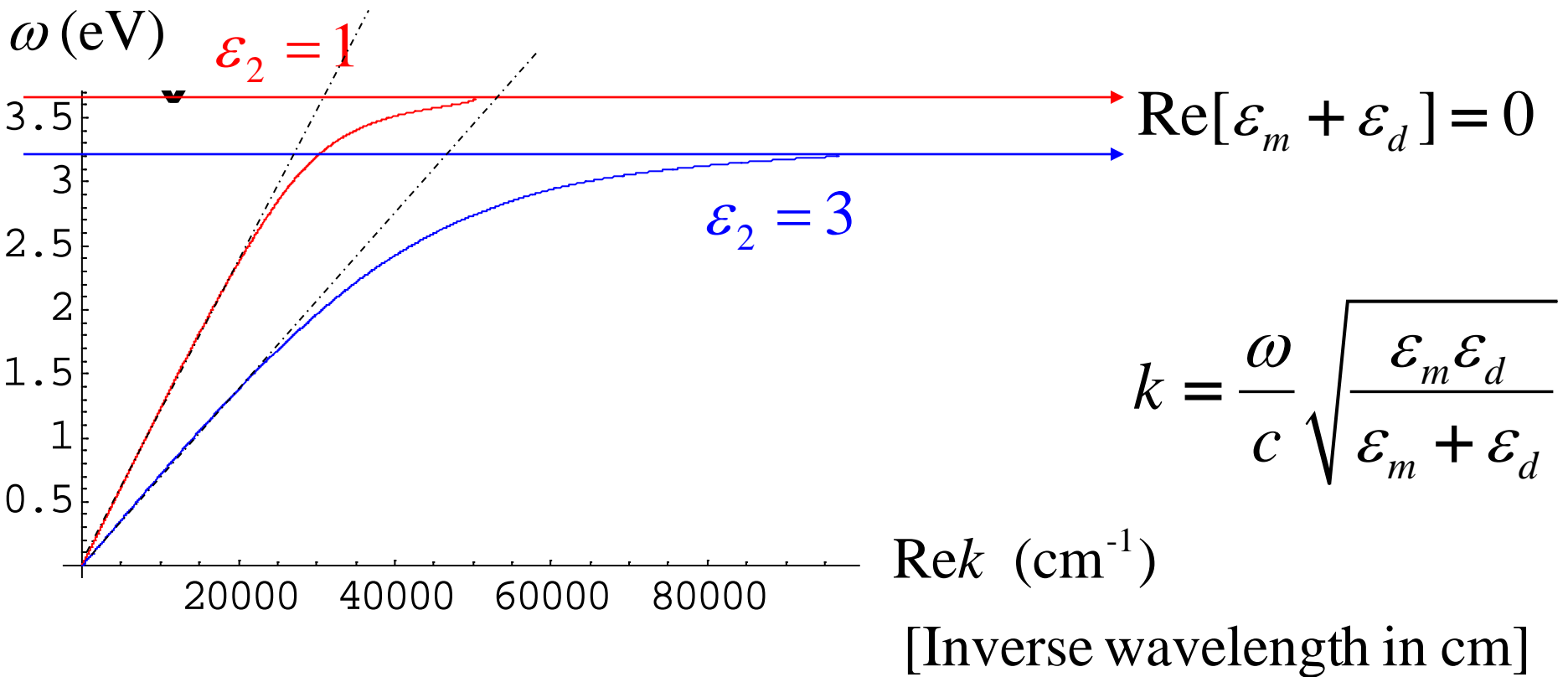
Im ϵ ; $\gamma = 0.055$ eV



ω (eV)

Fit to visible

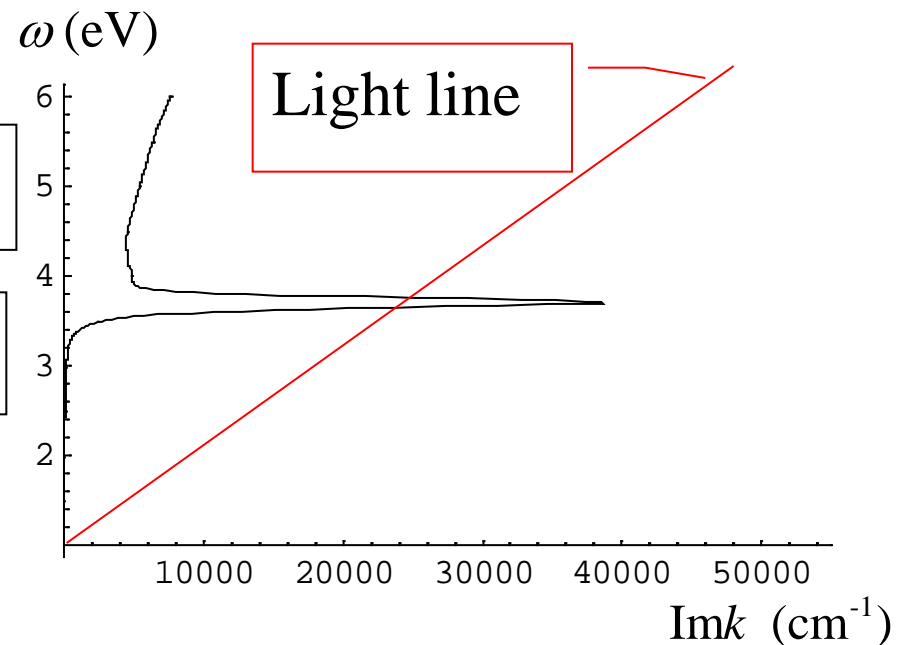
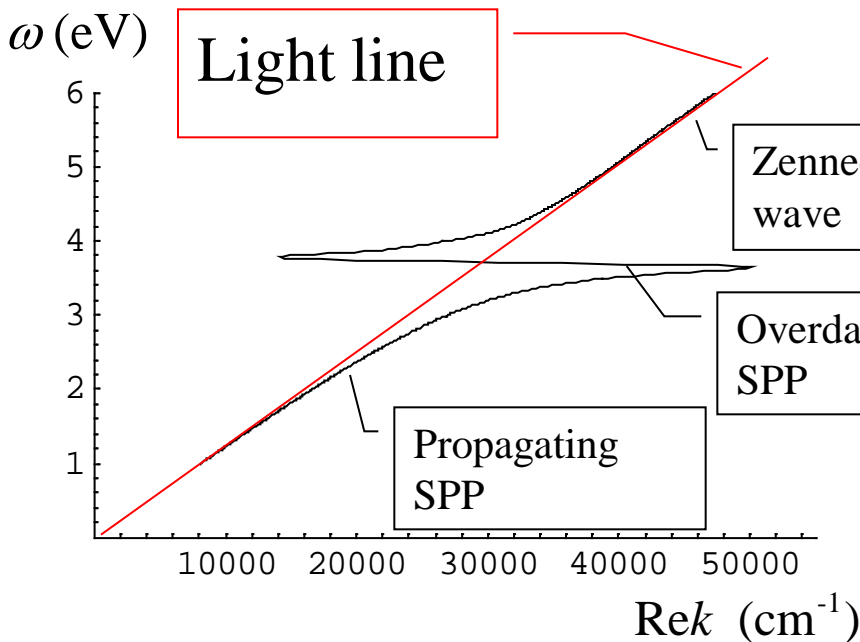
Surface plasmon dispersion and resonance for real silver [data of Johnson and Christy, P. B. Johnson and R. W. Christy, *Optical-Constants of Noble-Metals*, Phys. Rev. B 6, 4370-4379 (1972)]



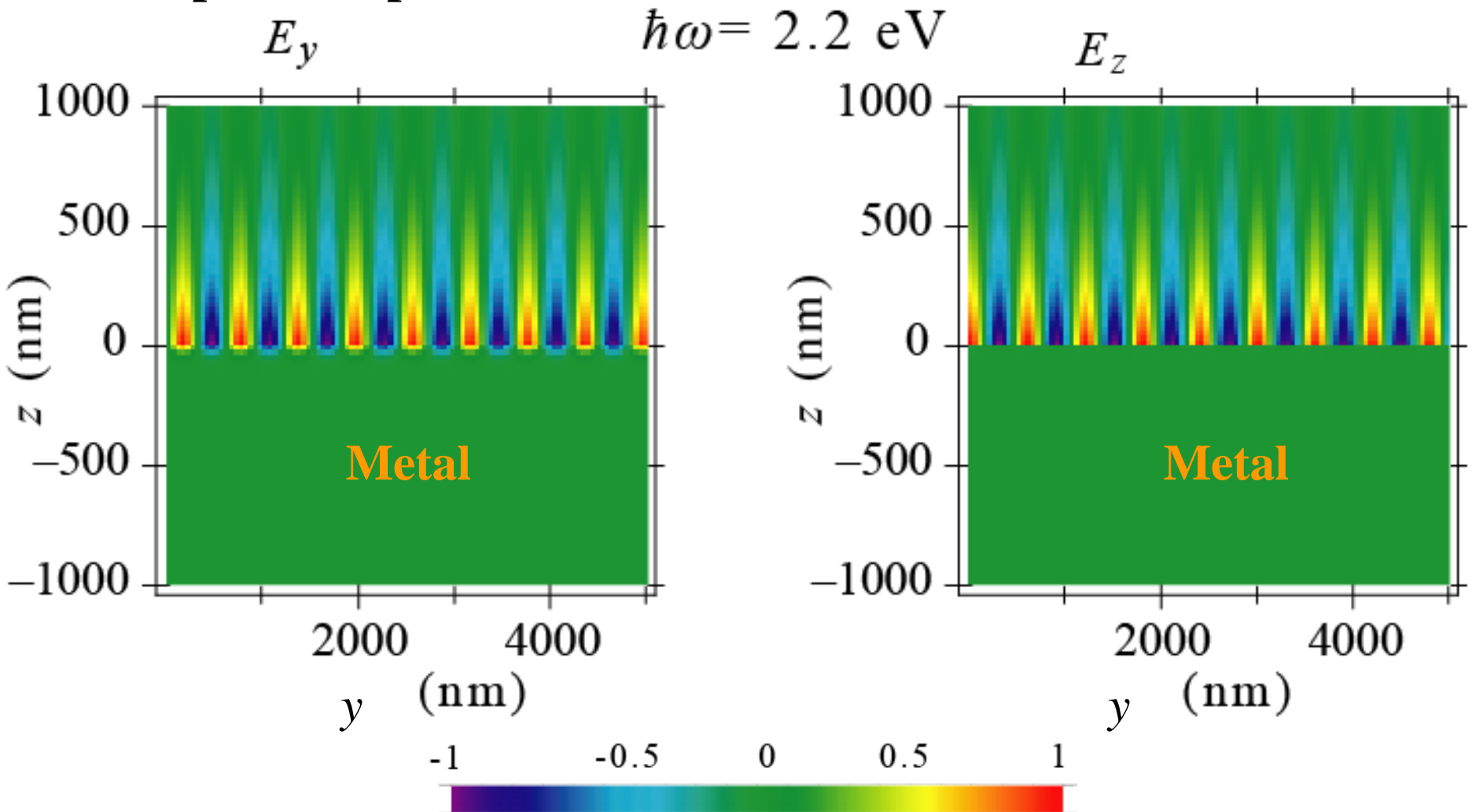
Surface Plasmon Polaritons and Sommerfeld-Zenneck Waves (example for silver in vacuum)

$$k = \frac{\omega}{c} \sqrt{\frac{\epsilon_m(\omega)}{\epsilon_m(\omega) + 1}}$$

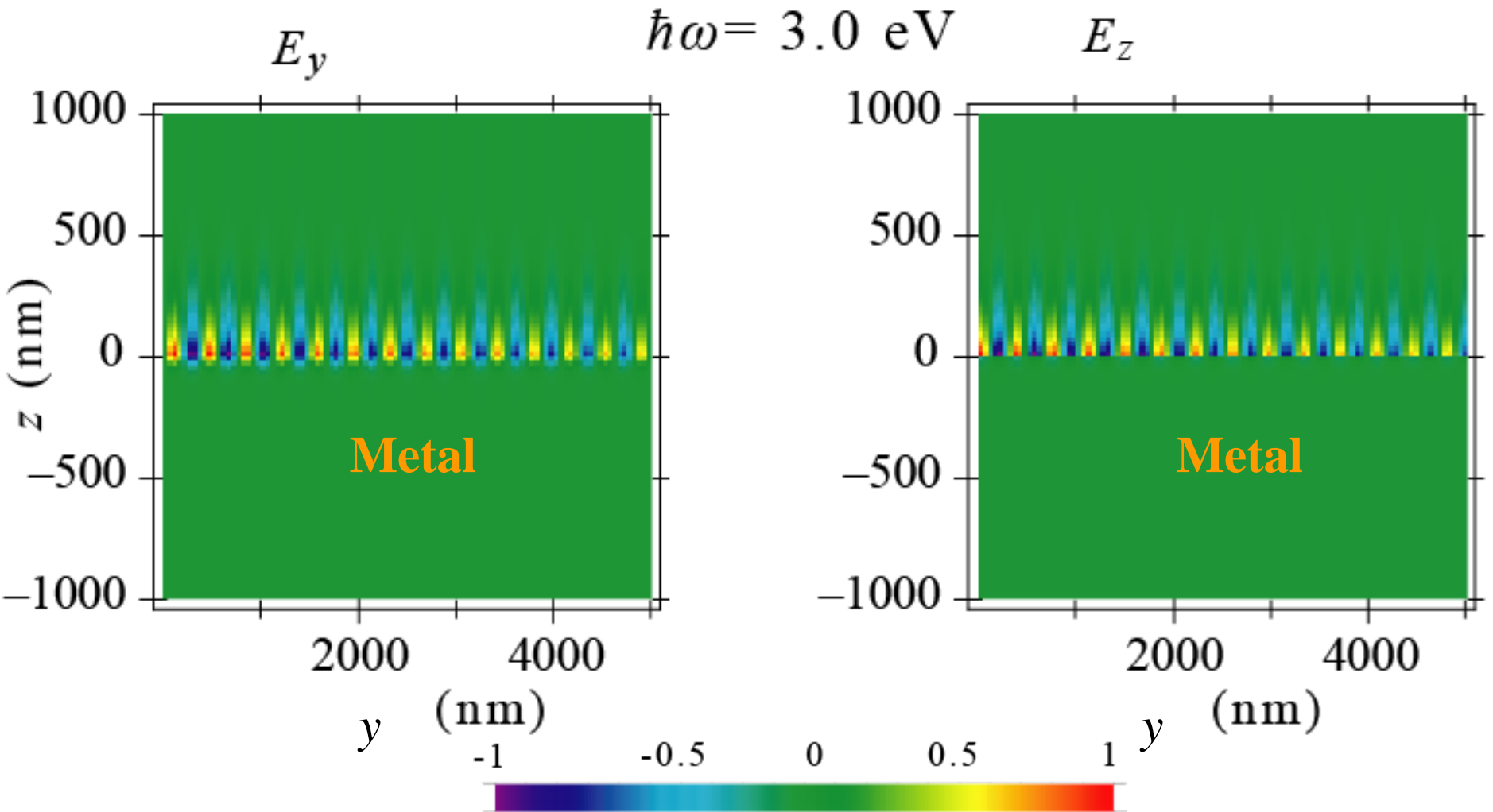
$$K_{\text{vacuum}} = \frac{\omega}{c} \sqrt{-\frac{1}{\epsilon_m(\omega) + 1}}$$



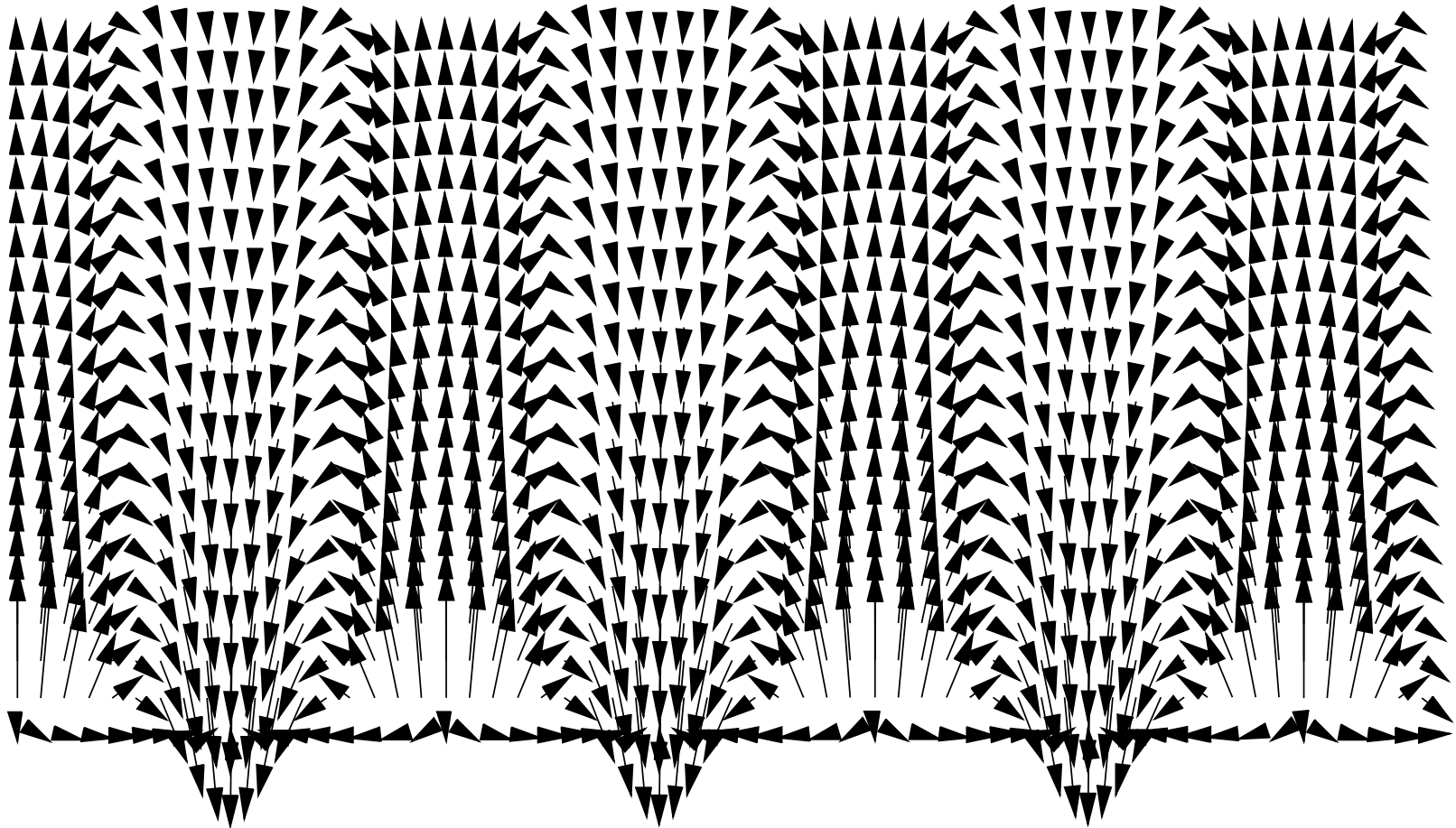
Surface plasmon polariton fields



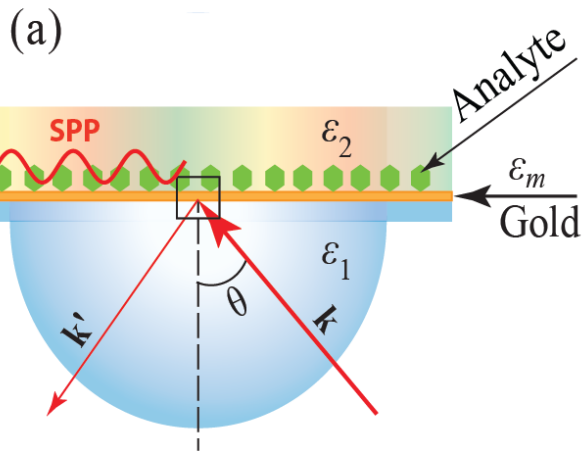
Surface plasmon polaritons fields



Topography of Surface Plasmon Polariton Electric Fields

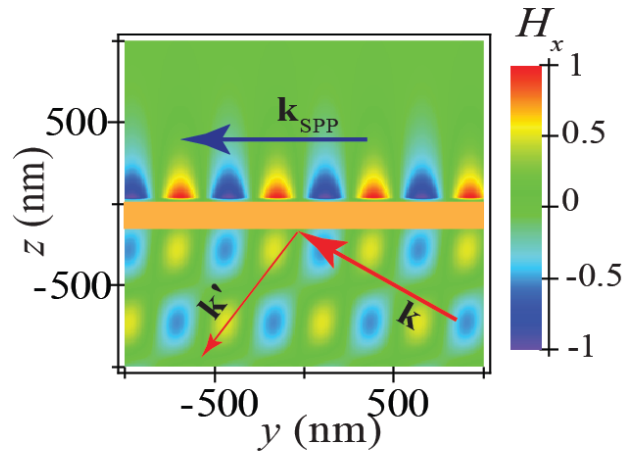


SPP excitation in Kretschmann geometry and SPP sensing

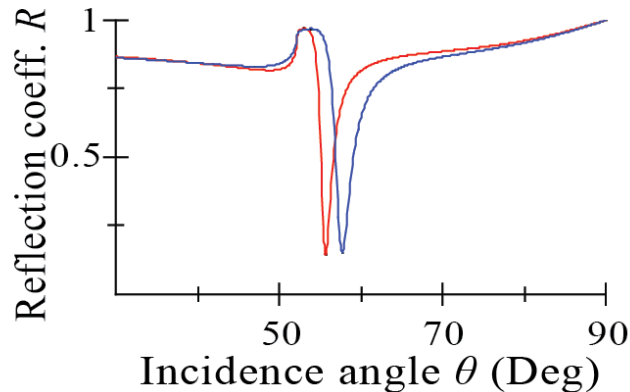


(b)

Sensors: <http://www.biacore.com/>



(c)



$$\sqrt{\epsilon_1} \sin \theta_K = \sqrt{\frac{\epsilon_m \epsilon_2}{\epsilon_m + \epsilon_2}}, \text{ where } \theta_K \text{ is Kretschmann angle}$$

$$\epsilon_1 > \frac{\epsilon_m \epsilon_2}{\epsilon_m + \epsilon_2} > \epsilon_2$$

$$\sqrt{\epsilon_1} \sin \theta_{TIR} = \sqrt{\epsilon_2}, \text{ where } \theta_{TIR} \text{ is total internal reflection angle}$$

$$\theta_K > \theta_{TIR}$$

Three-Layer Systems

Dispersion relation (exact analytical expression), where d is the layer thickness: defines the SPP wave vector k

$$\exp[2k_0 d \varepsilon_2 u_2] = \frac{(u_1 - u_2) \times (u_3 - u_2)}{(u_1 + u_2) \times (u_3 + u_2)}; \quad u_i = \frac{1}{\varepsilon_i} \sqrt{k^2 - \varepsilon_i}; \quad k_0 = \frac{\omega}{c}$$

Here ε_i is dielectric permittivity of i -th layer

Another form:

$$\tanh[k_0 d \varepsilon_2 u_2] = -\frac{u_2 (u_1 + u_3)}{u_1 u_3 + u_2^2}$$

Problem

Find quasistatic limit of the dispersion relation, which describes thin metal nanofilms and graphene embedded between two dielectrics. Obtain an explicit solution by applying the Drude formula $\epsilon_2 = -\omega_p^2 / \omega^2$. Finally, express through Fermi energy E_F of electrons (assuming a very low temperature $k_B T \ll E_F$).

Hint: Consider limit $k \gg k_0 \sqrt{|\epsilon_i|}$ while $kd \rightarrow 0$

$$\tanh[k_0 d \epsilon_2 u_2] = -\frac{u_2 (u_1 + u_3)}{u_1 u_3 + u_2^2}; \quad u_i = \frac{1}{\epsilon_i} \sqrt{\frac{k^2}{k_0^2} - \epsilon_i}; \quad k_0 = \frac{\omega}{c}$$

Solution to Problem

$$\tanh[k_0 d \varepsilon_2 u_2] = -\frac{u_2(u_1 + u_3)}{u_1 u_3 + u_2^2}; \quad u_i = \frac{1}{\varepsilon_i} \sqrt{\frac{k^2}{k_0^2} - \varepsilon_i}; \quad k_0 = \frac{\omega}{c}$$

$$u_i \approx \frac{1}{\varepsilon_i} \frac{k}{k_0}; \quad \tanh\left[k_0 d \varepsilon_2 \frac{1}{\varepsilon_2} \frac{k}{k_0}\right] \approx -\frac{\varepsilon_1 + \varepsilon_3}{\varepsilon_2} \rightarrow 0$$

Thus tanh can be expanded as $\tanh x \approx x$ yielding

$$k \approx -\frac{\varepsilon_1 + \varepsilon_3}{d \varepsilon_2(\omega)}.$$

Substituting $\varepsilon_2 = -\omega_p^2 / \omega^2$, we obtain SPP dispersion relation:

$$k \approx \frac{\omega^2}{\omega_p^2} \frac{\varepsilon_1 + \varepsilon_3}{d}, \text{ or } \omega = \omega_p \sqrt{\frac{kd}{\varepsilon_1 + \varepsilon_3}}$$

For 3D metal, $\omega_p = \sqrt{\frac{4\pi n e^2}{m}}$, thus $k = \frac{\omega^2 m}{4\pi n e^2} \frac{\epsilon_1 + \epsilon_3}{d}$.

Substituting relation between density and Fermi energy E_F ,

$n = \frac{m E_F}{\pi \hbar^2 d}$, we obtain $k = \hbar^2 \omega^2 \frac{\epsilon_1 + \epsilon_3}{4 e^2 E_F}$, or

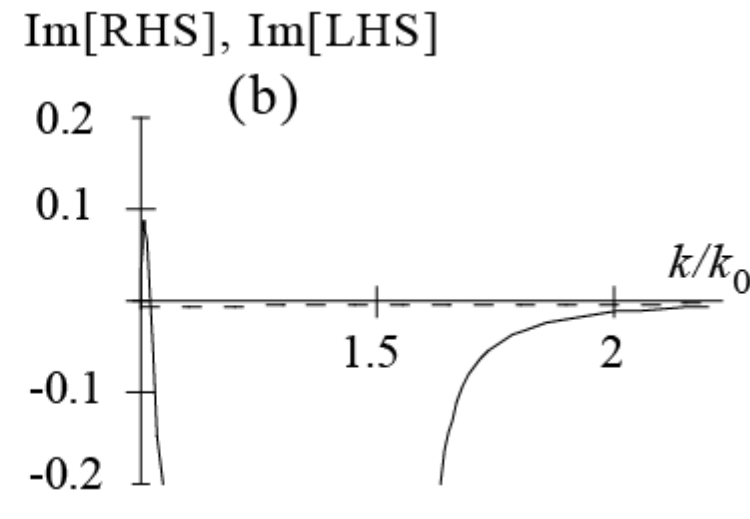
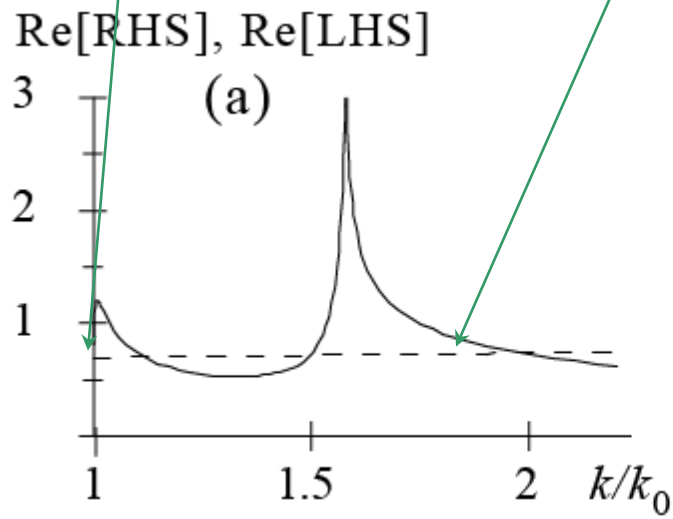
$k = \hbar^2 \omega(\omega + i\gamma) \frac{\epsilon_1 + \epsilon_3}{4 e^2 E_F}$ with collision rate γ .

For graphene in terms of E_F , the SPP dispersion relation can be shown to be exactly the same.

IMI Waveguide

Fast SPP root
 (Long range SPP)

Slow SPP root
 (Short range SPP)



Two roots for nano-thin silver in vacuum: Symmetric and Antisymmetric SPPs. No cut-off for SPP as thickness tends to zero

Dispersion Relations for Symmetric Systems

$$\varepsilon_1 = \varepsilon_3$$

$$\tanh[k_0 d \varepsilon_2 u_2] = -\frac{2u_1 u_2}{u_1^2 + u_2^2}; \quad \text{using: } \tanh 2x = \frac{2 \tanh x}{1 + \tanh^2 x}$$

Parity (symmetry) is conventionally defined as that of the *normal* (z) component of the electric field or the magnetic field (x -component)

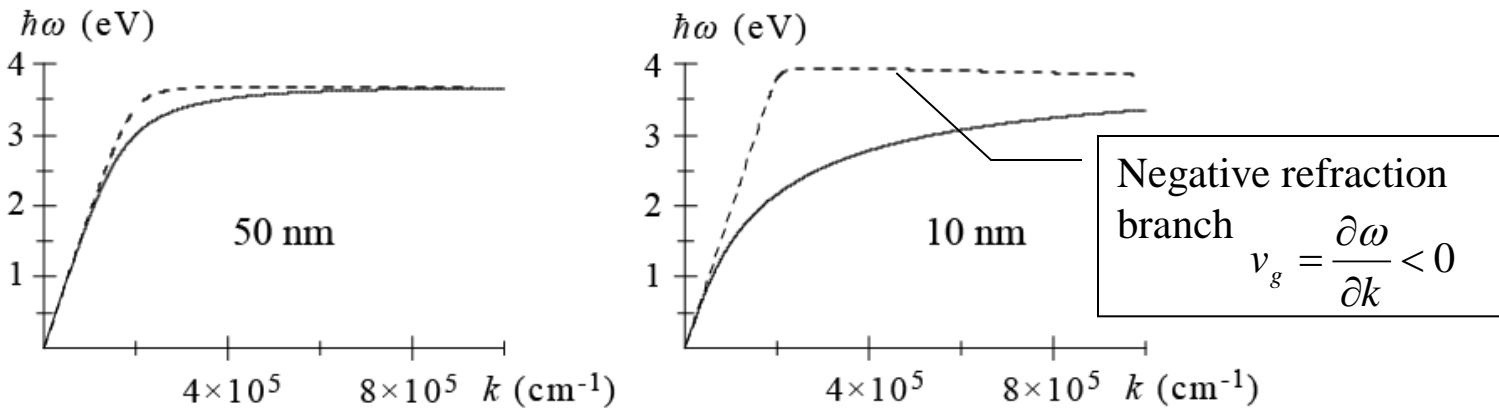
Even (symmetric) mode

Odd (antisymmetric) mode

$$\tanh\left[\frac{1}{2} k_0 d \varepsilon_2 u_2\right] = -\frac{u_1}{u_2}$$

$$\tanh\left[\frac{1}{2} k_0 d \varepsilon_2 u_2\right] = -\frac{u_2}{u_1}$$

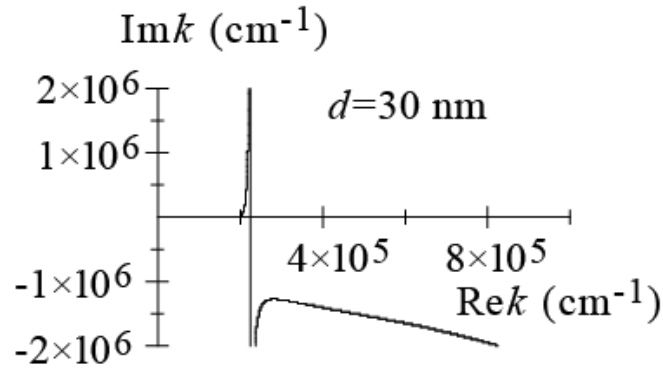
Dispersion relations for nanofilm of silver in vacuum (IMI structure):
 Symmetric mode (dashed) and antisymmetric mode (solid line)



Decay exponent (Imk) for 30 nm silver layer

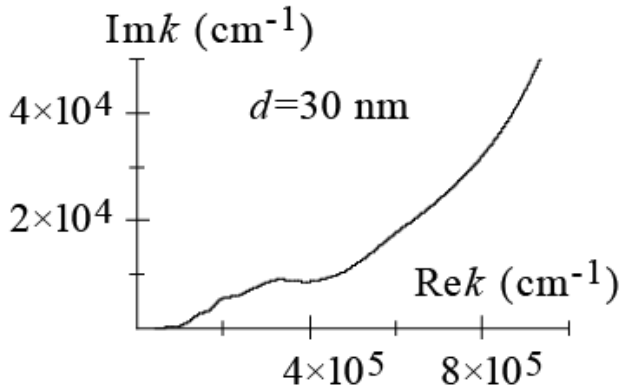
Symmetric mode

(a)

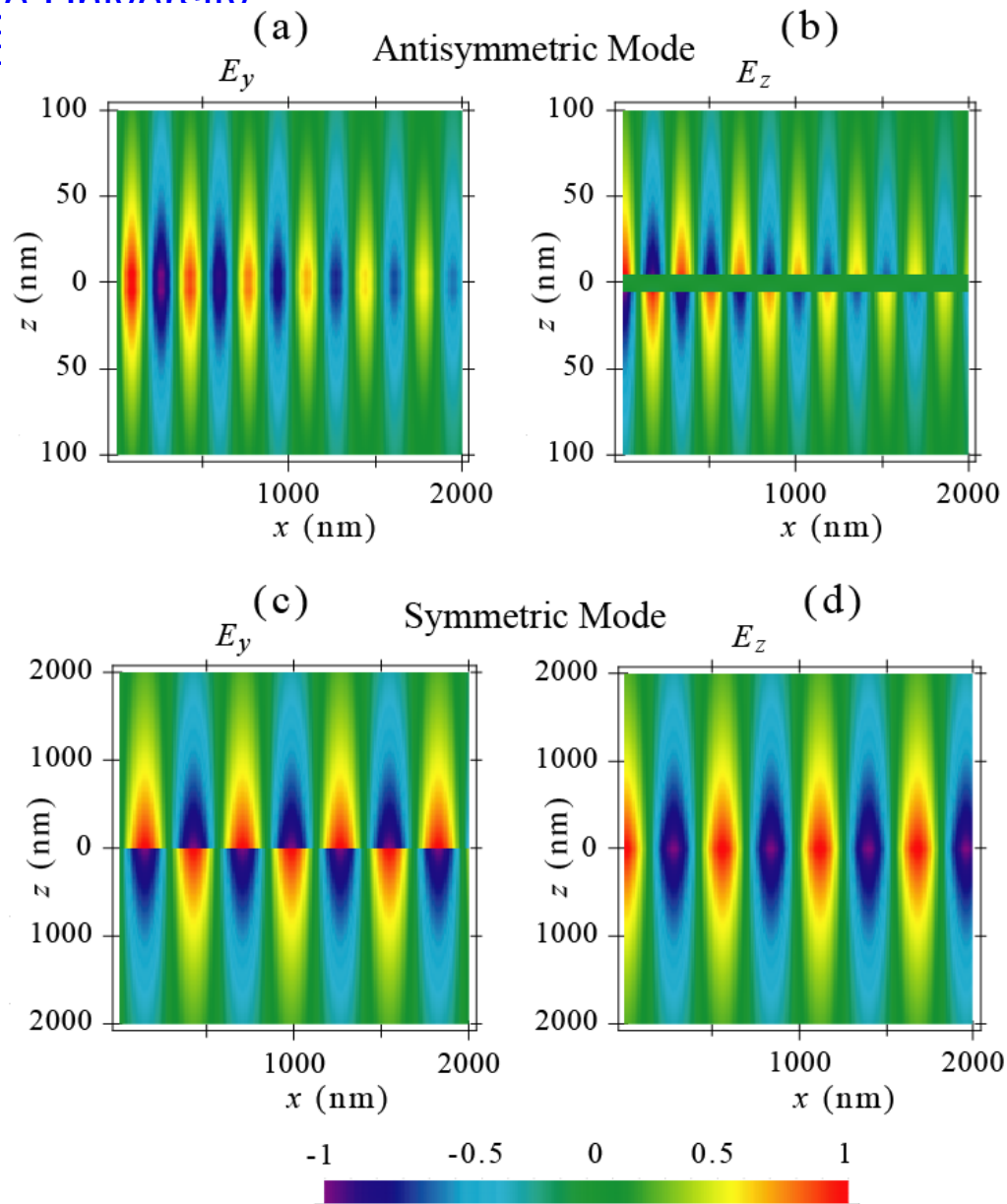


Antisymmetric mode

(b)



Local electric fields for 10 nm silver layer in vacuum at 2.2 eV frequency



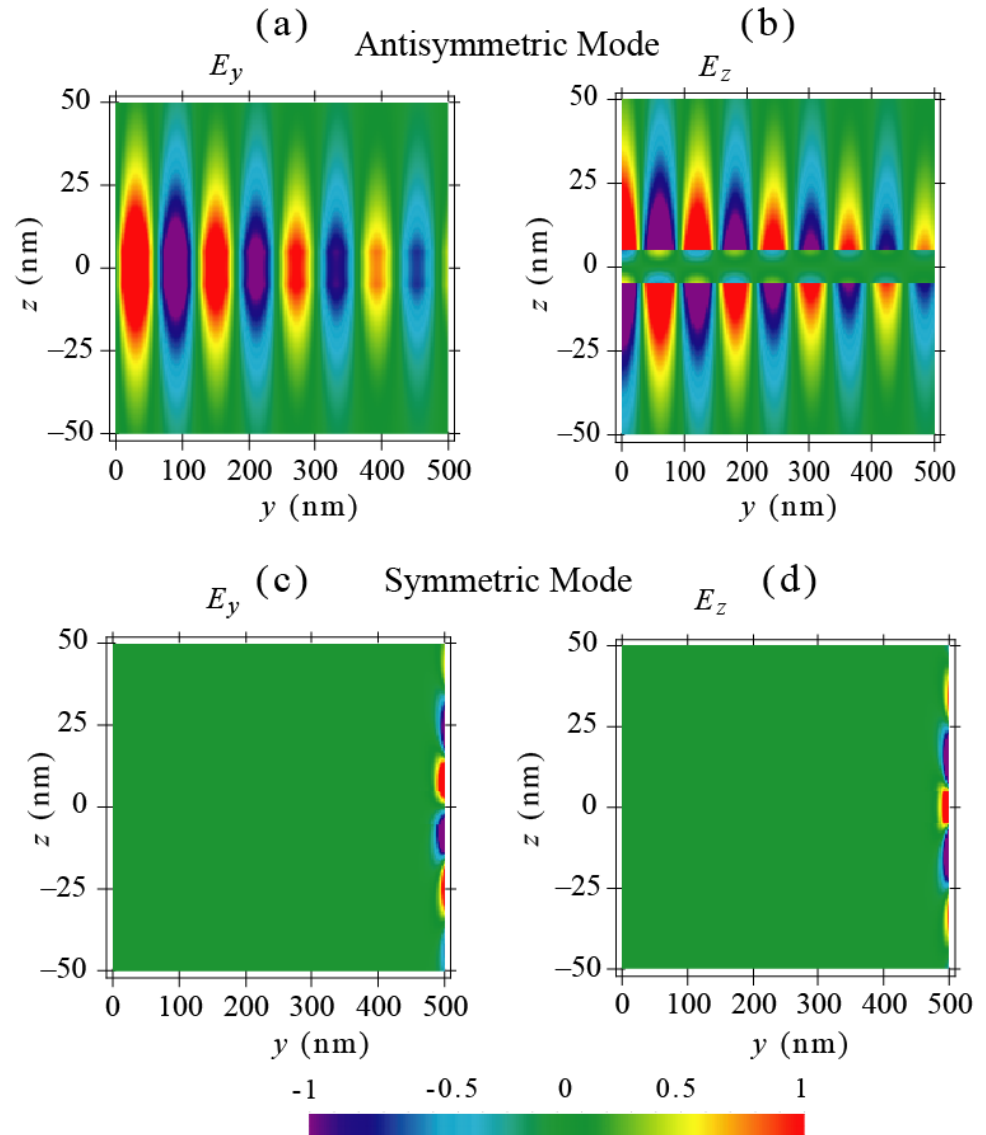
Local fields for 10 nm layer of silver in vacuum for a high wave vector

$$\text{Re}k = 5 \cdot 10^5 \text{ cm}^{-1}$$

Antisymmetric mode: positive refraction

Symmetric mode: negative refraction, high loss (practically, no propagation).

The sign of refraction is determined by the sign of the group velocity $v_g = \frac{\partial \omega}{\partial k}$

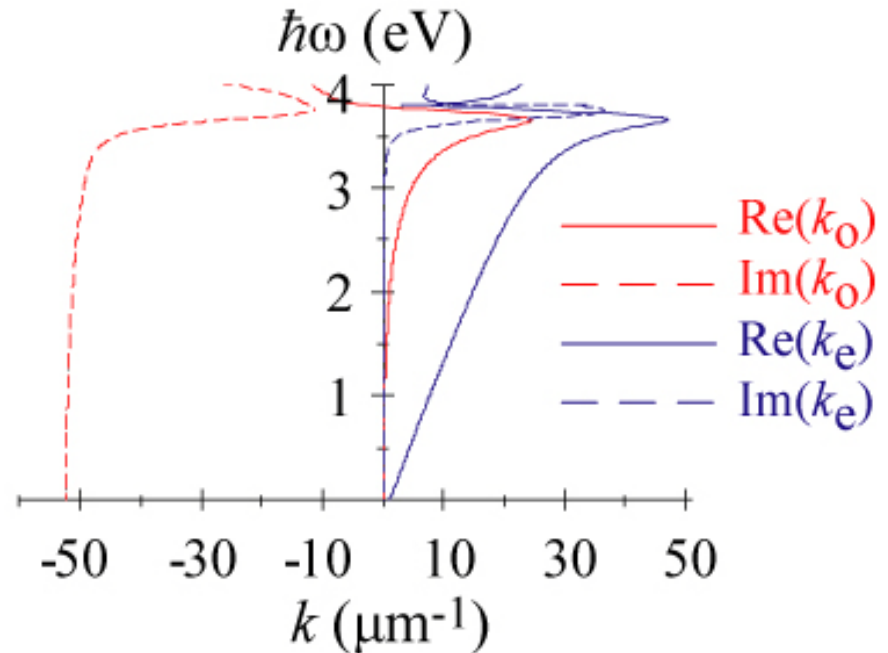


SPPs in Metal-Insulator-Metal Waveguides

$\epsilon_m(\omega)$

ϵ_d

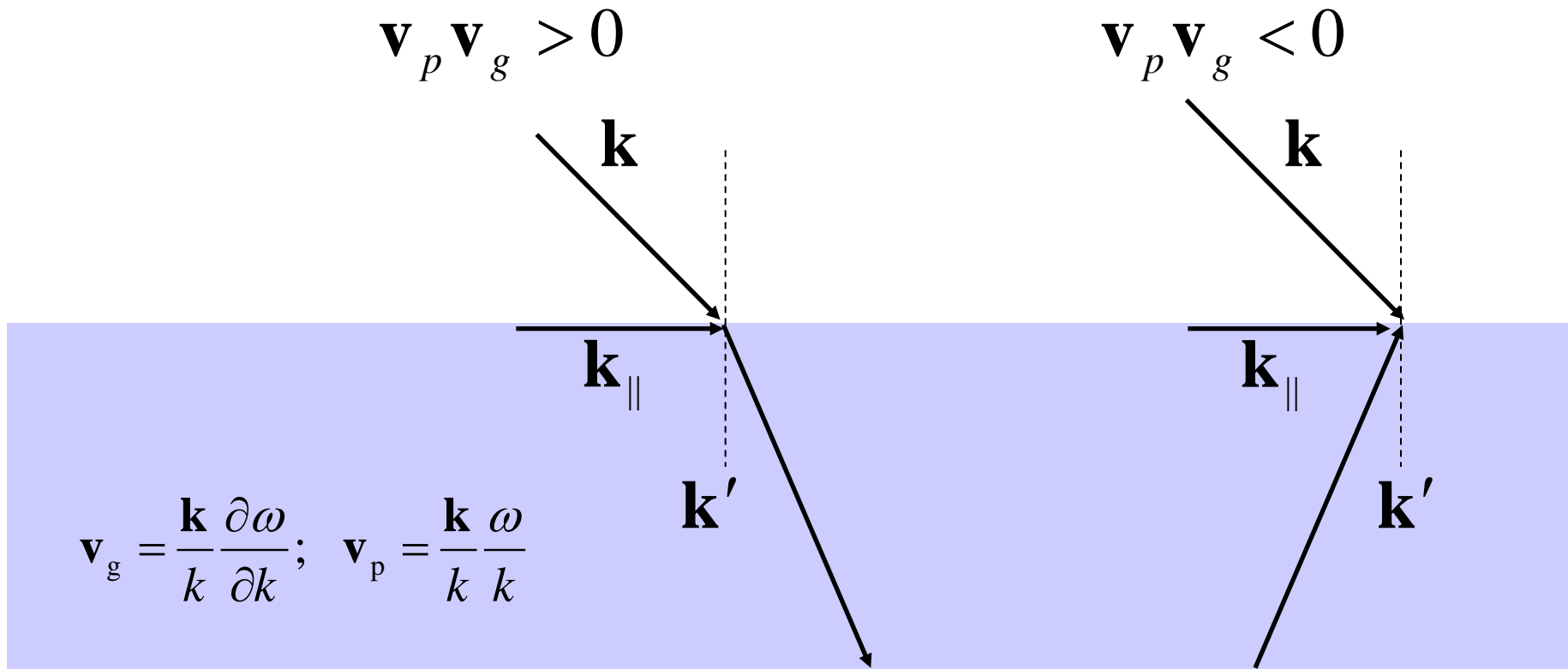
$\epsilon_m(\omega)$



for **odd (antisymmetric) mode**: $\text{Im } k_o \cdot \text{Re } k_o < 0 \Rightarrow$ negative refraction

for **all modes**: $\text{Re } k_o \leq |\text{Im } k_o| \Rightarrow$ large dissipation

Radiative condition (other “causality”): Selecting one of the two solutions in electrodynamics. Mandelstam-Veselago’s negative refraction



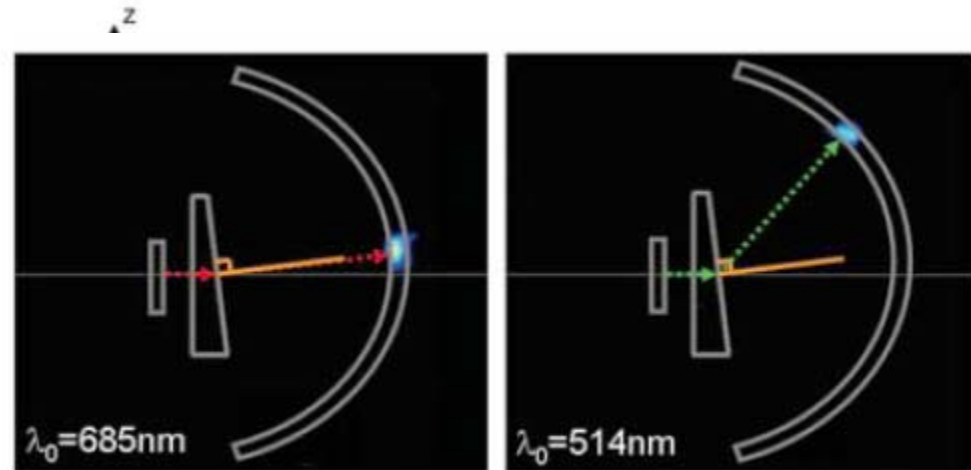
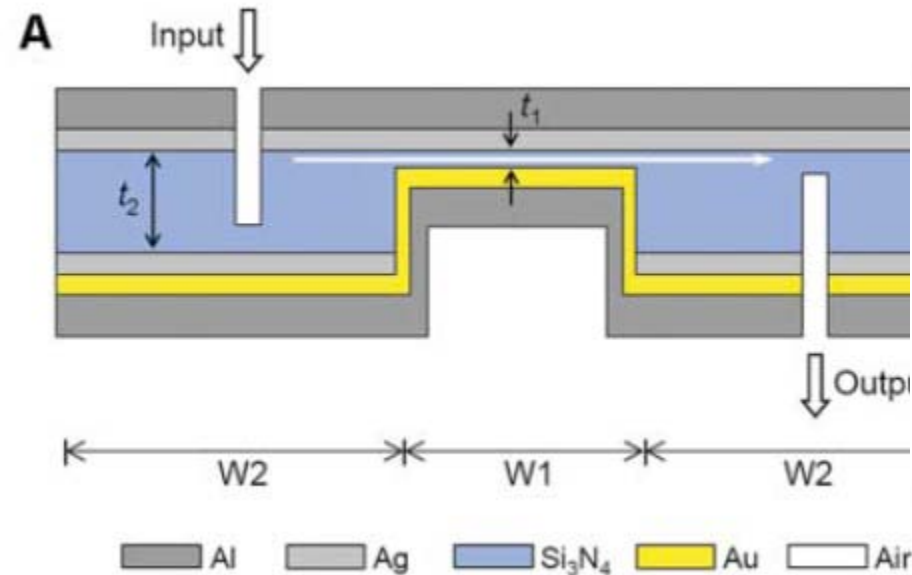
Universal negative refraction condition from causality : $\text{Im} \mathbf{k} \cdot \text{Re} \mathbf{k} < 0$

REPORTS

Negative Refraction at Visible Frequencies

20 APRIL 2007 VOL 316 SCIENCE

Henri J. Lezec,^{1,2*†} Jennifer A. Dionne,^{1*} Harry A. Atwater¹





Criterion for Negative Refraction with Low Optical Losses from a Fundamental Principle of Causality

Mark I. Stockman*

General condition of negative refraction in isotropic medium (does not depend on choice of the square root sign for n):

$$\text{Im } n^2 < 0 \quad \text{or} \quad \text{Im } n \cdot \text{Re } n < 0 \quad \text{or} \quad \text{Im } \mathbf{k} \cdot \text{Re } \mathbf{k} < 0;$$

$$\text{Im } n^2 \equiv \text{Re } \varepsilon \text{Im } \mu + \text{Re } \mu \text{Im } \varepsilon.$$

Group velocity is the transfer of energy velocity only if losses are small enough.

If losses at the observation frequency are zero, then an exact causality relation is valid for isotropic medium without spatial dispersion:

$$\frac{c^2}{\mathbf{v}_p \cdot \mathbf{v}_g} = 1 + \frac{2}{\pi} \int_0^\infty \frac{\text{Im } n^2(\omega_1)}{(\omega_1^2 - \omega^2)^2} d\omega_1, \text{ where } \omega \text{ is the observation frequency}$$

Criterion of negative refraction without loss at the observation frequency is

$$\int_0^\infty \frac{\text{Im } n^2(\omega_1)}{(\omega_1^2 - \omega^2)^2} d\omega_1 < -\frac{\pi}{2}$$

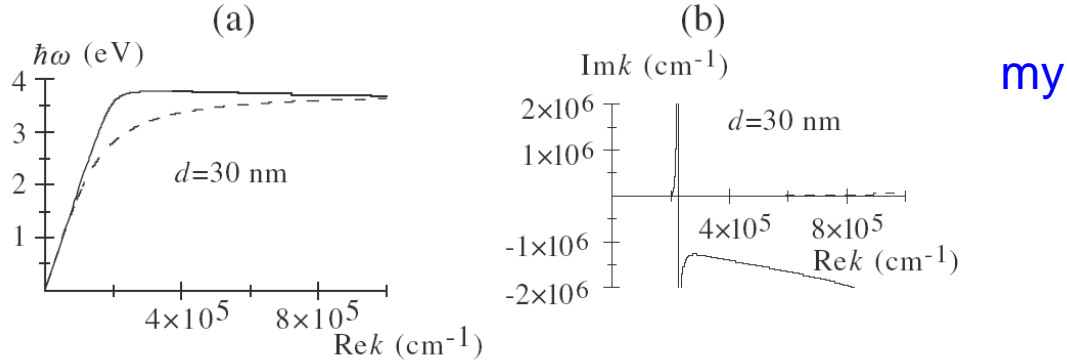


FIG. 1. Dispersion relations for thin silver film in vacuum. The symmetric and antisymmetric modes are displayed with solid and dashed lines, respectively. (a) Real part of dispersion relation: frequency ω as a function of $Re k$. (b) Imaginary part of the dispersion relation: dependence of $Im k$ on $Re k$. Thickness of the silver film is $d = 30$ nm.

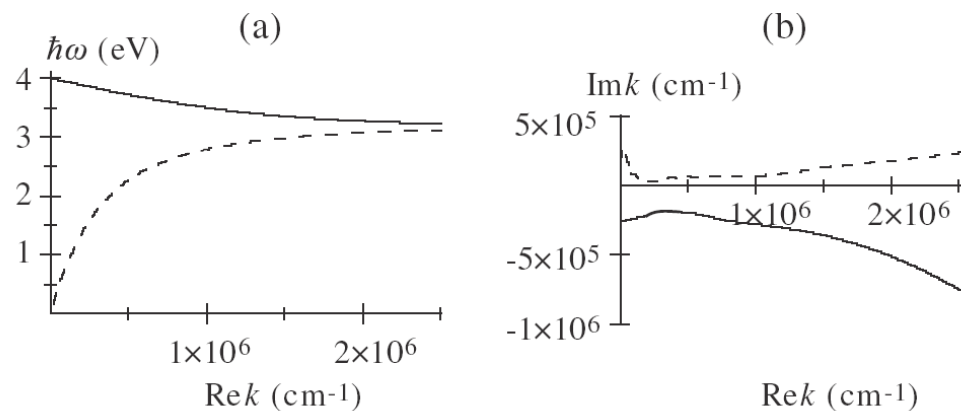


FIG. 2. (a) For a thin ($d = 10$ nm) dielectric layer with $\epsilon_d = 3$ embedded in silver, dispersion relation of SPPs is displayed as dependence of frequency $\hbar\omega$ on the real part of wave vector. (b) For the same system, dependence of $Im k$ on $Re k$. For both panels, the solid lines pertain to the antisymmetric SPP mode, and the dashed lines denote the symmetric SPP mode.

CONCLUSIONS

1. In metal/dielectric layered systems there exist surface plasmon polariton (SPP) modes of different symmetries
2. For a metal layer in a dielectric medium, there are two types of SPP: symmetric (fast or long-range) SPP and antisymmetric (slow or short-range) SPP
3. Slow SPP for a thin metal film is nanolocalized at the surface of the film. It is useful to couple nanosystems to laser sources.
4. There is no cut-off as SPP wavelength tends to infinity.
5. Losses of negative refraction (back-propagating SPP) are very large
6. To have negative refraction without loss at an observation frequency, there must be loss in the adjacent region of negative refraction

Adiabatic Nano-Optics

Conventional (non-adiabatic) conversion to the near zone (direct excitation of local, near-zone fields by far-zone radiation) is very energy-inefficient, though can generate high local fields.

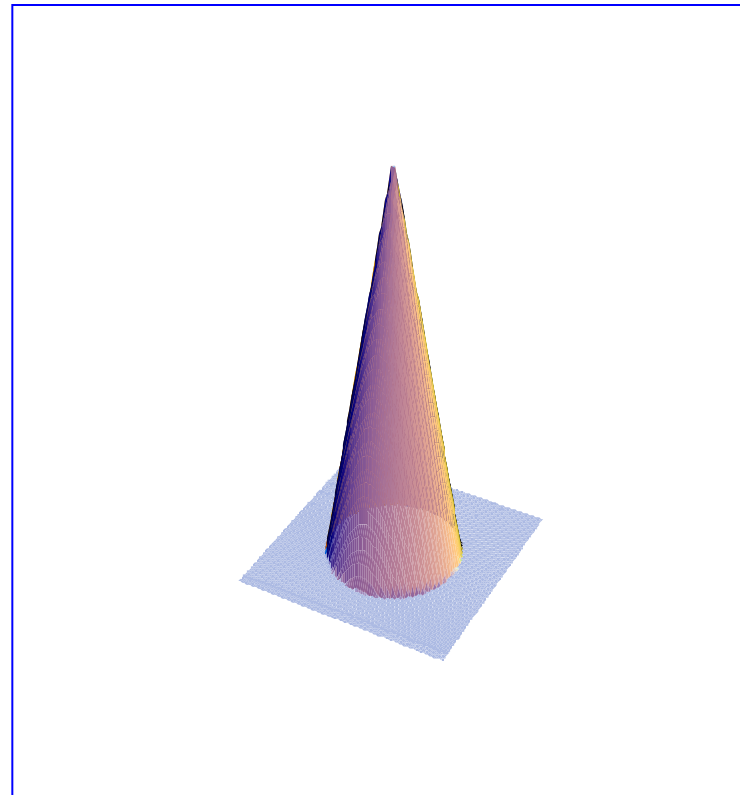
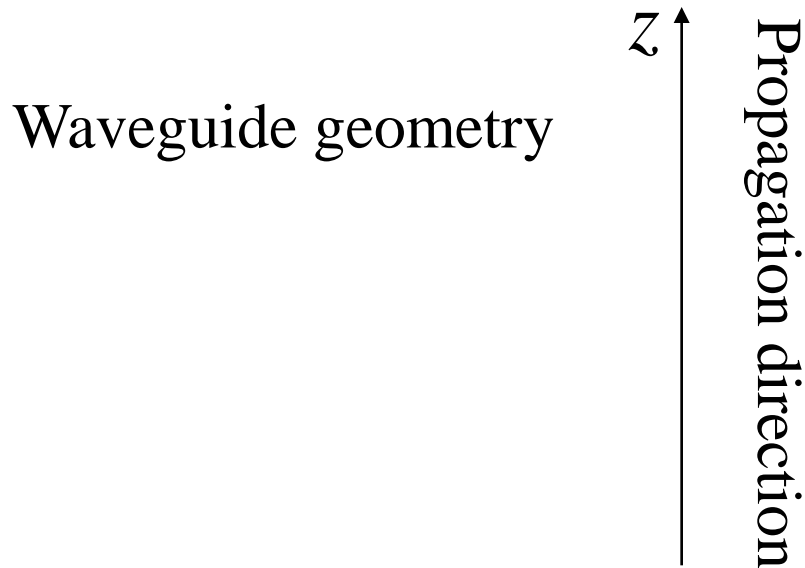
Both aperture and aperturless methods lead to loss of the major fraction of energy. If one could focus optical radiation from the far zone to nanoscale region, then the problem of the energy-efficient excitation of the local fields would have been solved. However, it is commonly known that it is impossible

Is it? We show that this common wisdom is wrong.

Using *adiabatic* transformation, one can transfer energy from the far zone to near field without major losses, with a high efficiency, limited only by absorption in plasmonic waveguides.

Adiabatic Nanofocusing of Surface Plasmon Polaritons

M. I. Stockman, *Nanofocusing of Optical Energy in Tapered Plasmonic Waveguides*, Phys. Rev. Lett. **93**, 137404-1-4 (2004).



Electric field of SPP wave for TM_0 mode (magnetic field is tangential to the surface, normal to the axis; axially-symmetric solution of the Maxwell curl equations)

$$r < R: E_z = I_0(\kappa_m r) \exp(ikz)$$

$$r > R: E_z = \frac{I_0(\kappa_m R)}{K_0(\kappa_d R)} K_0(\kappa_d r) \exp(ikz)$$

$$r < R: E_r = \frac{ik}{\kappa_m} I_1(\kappa_m r) \exp(ikz)$$

$$r > R: E_r = \frac{ik}{\kappa_d} \frac{I_0(\kappa_m R)}{K_0(\kappa_d R)} K_1(\kappa_d r) \exp(ikz)$$

Continuity of displacement at the surface:

$$\frac{\epsilon_m}{\kappa_m} I_1(\kappa_m R) = \frac{\epsilon_d}{\kappa_d} \frac{I_0(\kappa_m R)}{K_0(\kappa_d R)} K_1(\kappa_d R)$$

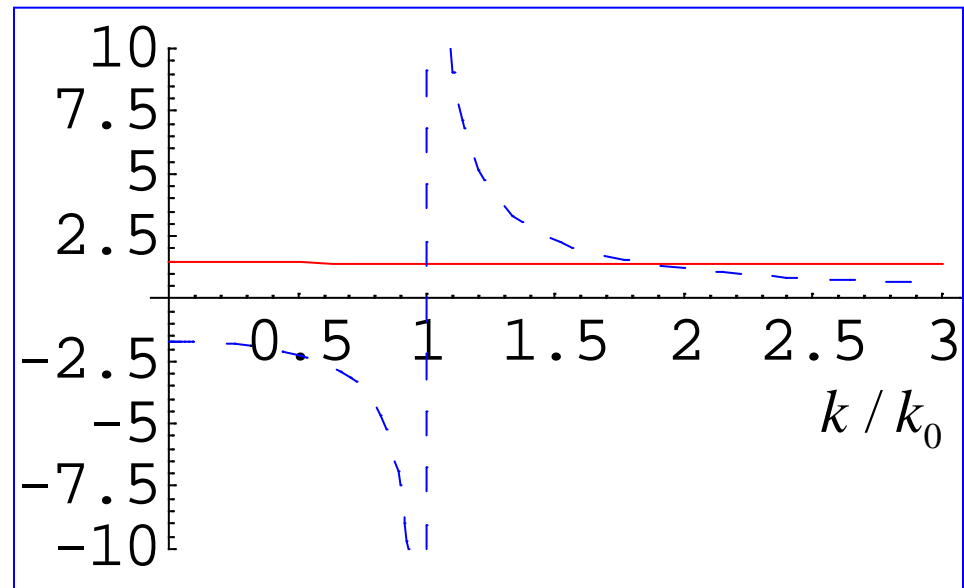
For TM₀ mode (magnetic field is tangential to the surface, normal to the axis; axially-symmetric solution), dispersion relation is

$$\frac{\varepsilon_m I_1(k_0 R \sqrt{k^2 - \varepsilon_m})}{\sqrt{k^2 - \varepsilon_m} I_0(k_0 R \sqrt{k^2 - \varepsilon_m})} = - \frac{\varepsilon_d K_1(k_0 R \sqrt{k^2 - \varepsilon_d})}{\sqrt{k^2 - \varepsilon_d} K_0(k_0 R \sqrt{k^2 - \varepsilon_d})}$$

$$k_0 = \frac{\omega}{c}$$

There is single root:

Slow SPP. There is no cutoff as its wavelength tends to zero (or wavevector tends to infinity)



Introduce effective index: $k = n\omega/c$

Close to the tip ($R \rightarrow 0$), this effective index diverges as $1/R$:

$$n(R) \approx \frac{1}{k_0 R} \sqrt{\frac{4\varepsilon_d}{-\varepsilon_m \log \frac{-4\varepsilon_m}{\varepsilon_d} - \gamma}}, \quad \gamma \approx 0.57721$$

This describes slowing down and asymptotic stopping of SPP. Important, the time to travel to the tip (singularity) of the conic waveguide logarithmically diverges,

$$t = \frac{1}{c} \int_{R_{\max}}^R n(r) dr \sim -\ln(k_0 R) \rightarrow \infty$$

Adiabatic parameter: $\delta = R' \frac{d\tilde{\lambda}(R)}{dR}$

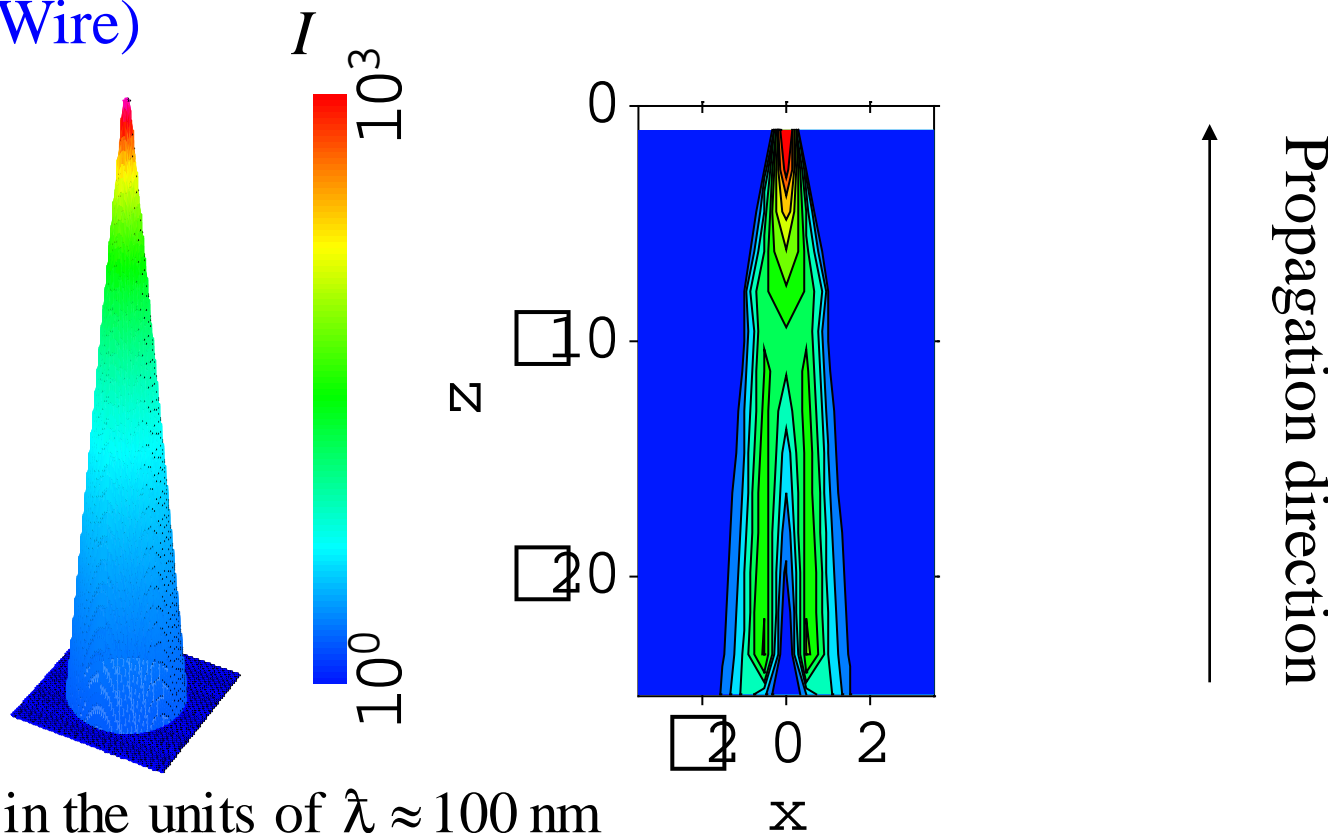
where $R' = \frac{dR(z)}{dz}$ is the waveguide grading

For a plasmonic (TM₀) mode, close to the tip

$$\delta \approx \left| R' \sqrt{-\frac{\epsilon_m}{2\epsilon_d}} \left[\ln \sqrt{-\frac{4\epsilon_m}{\epsilon_d}} - \gamma \right] \right|$$

Thus, adiabatic parameter stays finite everywhere, including the tip. Correspondingly, the adiabatic (eikonal or WKB) approximation is applicable uniformly over the entire tip.

Intensity of Local Fields at the Surface of Tapered Plasmonic Waveguide (Conic Silver Wire)



Coordinates are in the units of $\lambda \approx 100$ nm

M. I. Stockman, *Nanofocusing of Optical Energy in Tapered Plasmonic Waveguides*, Phys. Rev. Lett. **93**, 137404-1-4 (2004).

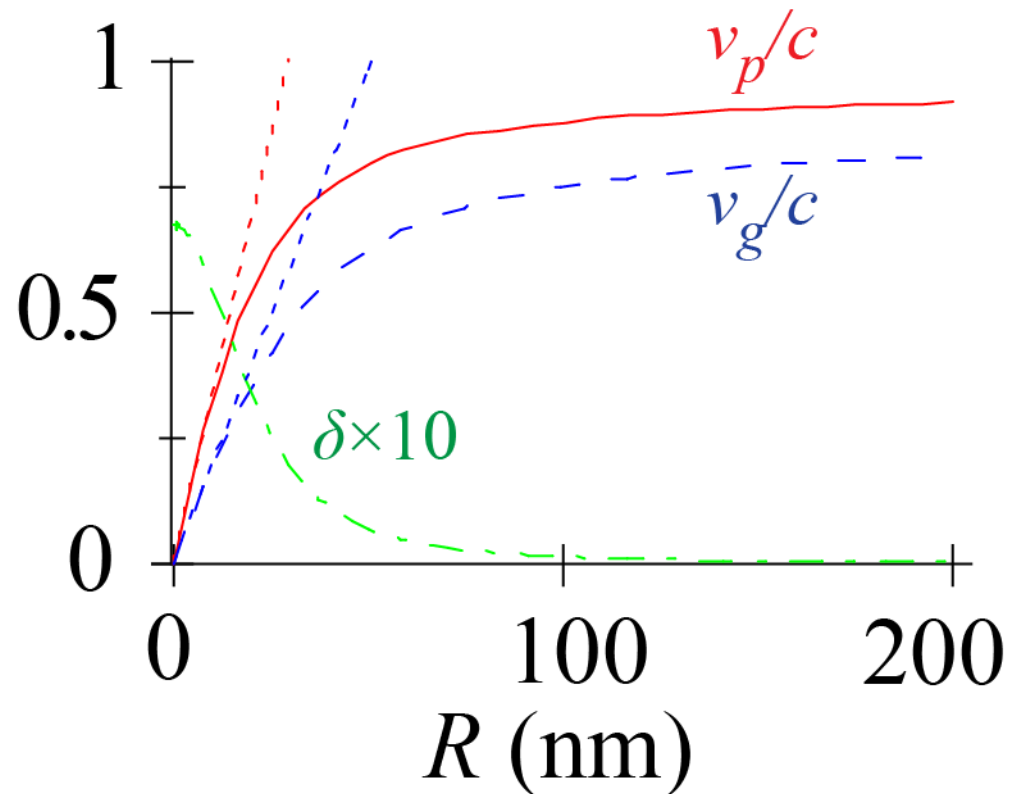
Phase velocity of surface plasmon polaritons

Group velocity of surface plasmon polaritons

Adiabatic parameter (scaled by 10)

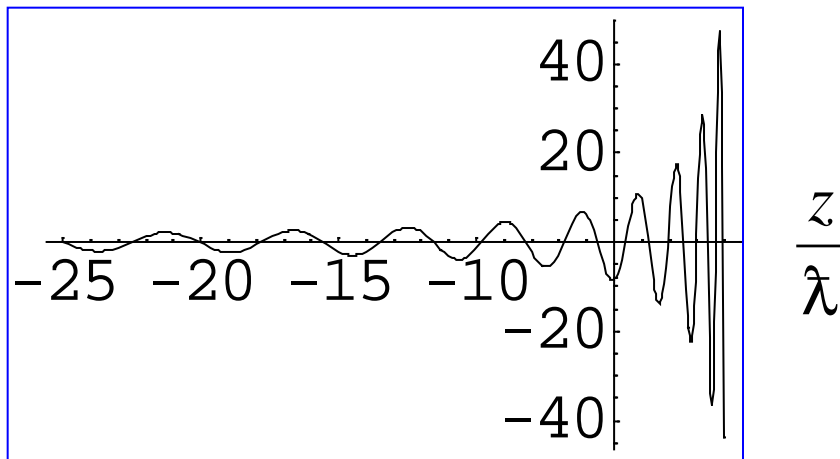
$$k(R) \approx \frac{1}{R} \sqrt{\frac{2\varepsilon_d}{-\varepsilon_m} \frac{1}{\frac{1}{2} \log \frac{-4\varepsilon_m}{\varepsilon_d} - \gamma}}$$

$$v_p = \left(\frac{k}{\omega}\right)^{-1} \propto R, \quad v_g = \left(\frac{\partial k}{\partial \omega}\right)^{-1} \propto R$$

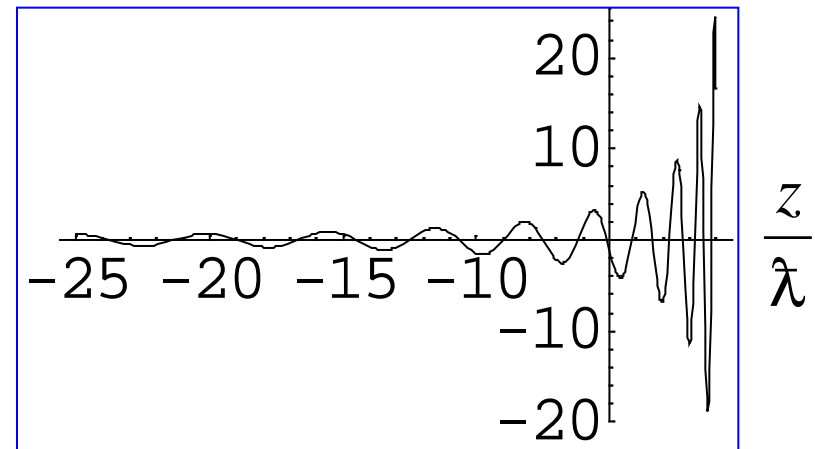


Local Electric Fields at Surface of Plasmonic Tapered Waveguide

Transverse field



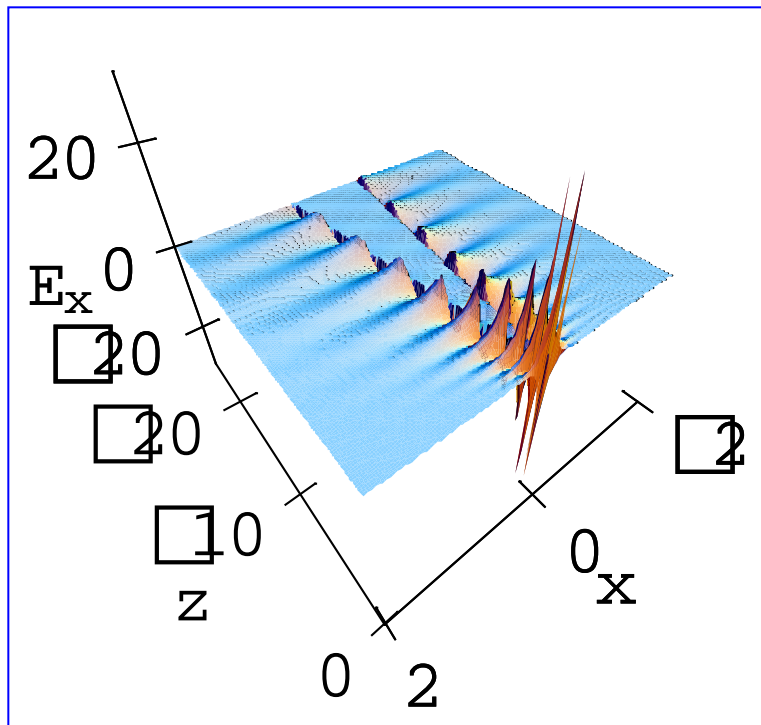
Longitudinal field



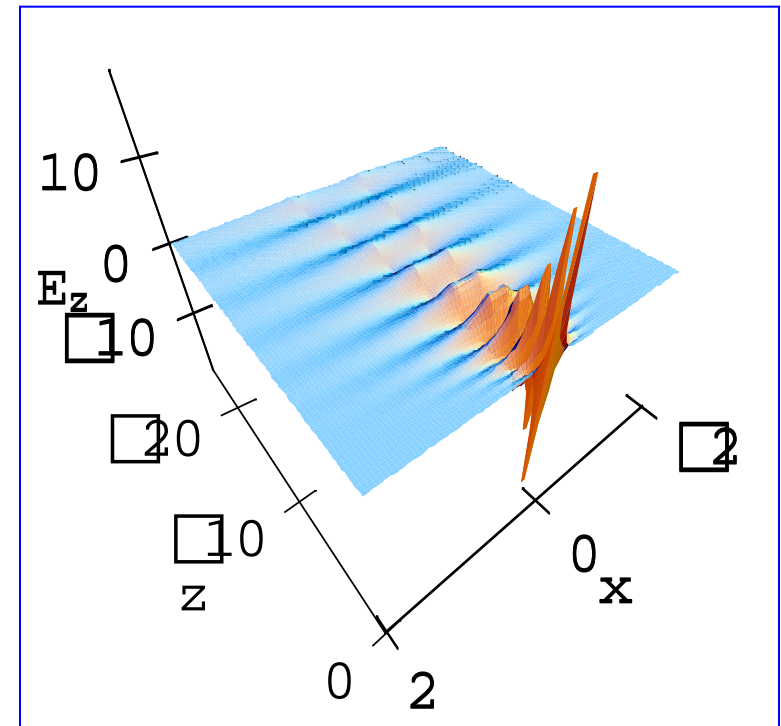
$\lambda \approx 100 \text{ nm}$

Local Electric Fields in Cross Section of System

Transverse electric field

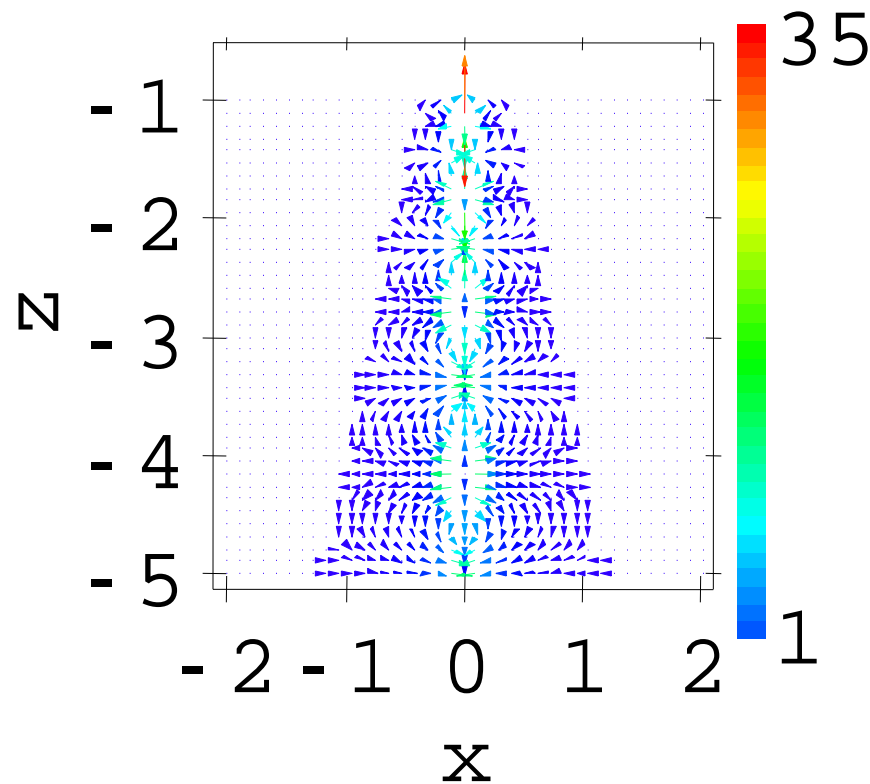


Longitudinal electric field



Coordinates are in the units of $\lambda \approx 100$ nm

Vector of optical electric field for TM_0 plasmonic mode of conic waveguide made of silver



Spatial scales are
in units of 100 nm

Problem

Analytically estimate field at the apex as a function of the distance to the apex.

Hint: Neglect losses and use energy conservation along the SPP propagation length.

Solution to Problem

Distance to the apex z and local radius R are proportional, $z \propto R$.

SPP wave vector is $k \propto R^{-1}$.

The field localization radius is $\Delta r \propto k^{-1} \propto R \propto z$.

The SPP group velocity is $v_g \propto R \propto z$.

Conservation of energy flux is $E^2 v_g R^2 \propto 1$, or

$E^2 z^3 \propto 1$. Correspondingly, $E^2 \propto z^{-3}$ is the field scaling.

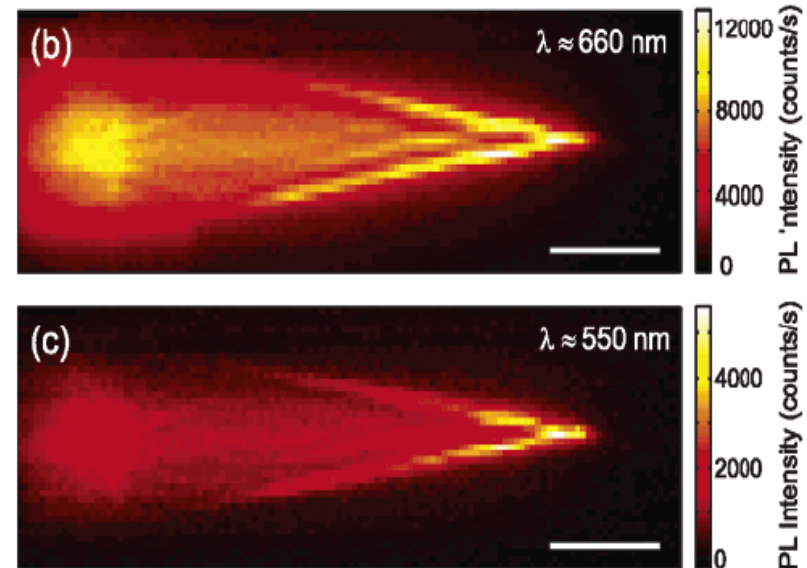
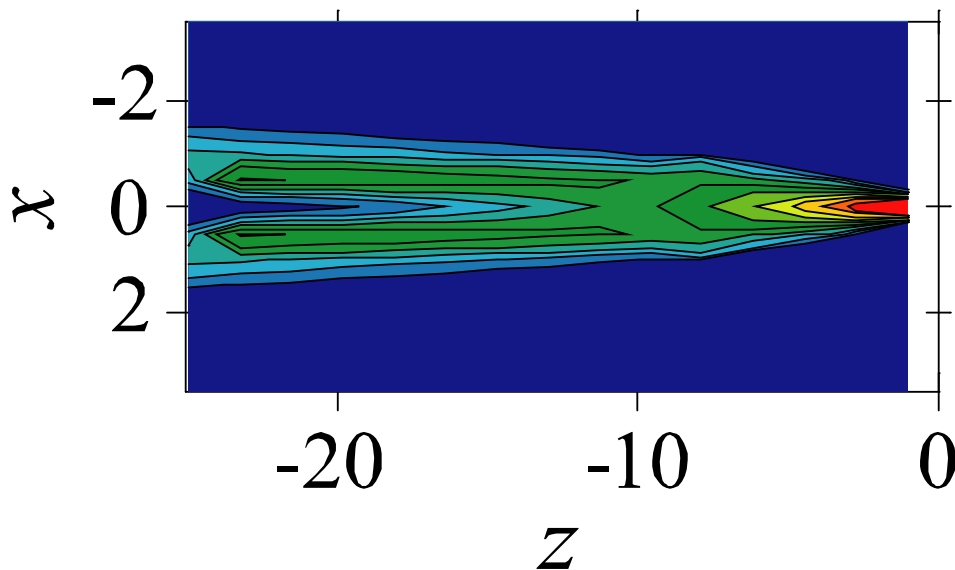
Enhanced Nonlinear Optical Effects with a Tapered Plasmonic Waveguide

Ewold Verhagen,* Laurens Kuipers, and Albert Polman

*Center for Nanophotonics, FOM Institute for Atomic and Molecular Physics (AMOLF),
Kruislaan 407, 1098 SJ Amsterdam, The Netherlands*

Nano Lett. **7**, 334-337 (2007)

(a)



Latest: E. Verhagen, A. Polman, and L. Kuipers, *Nanofocusing in Laterally Tapered Plasmonic Waveguides*, Opt. Express **16**, 45-57 (2008)

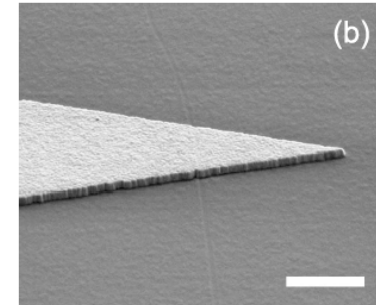
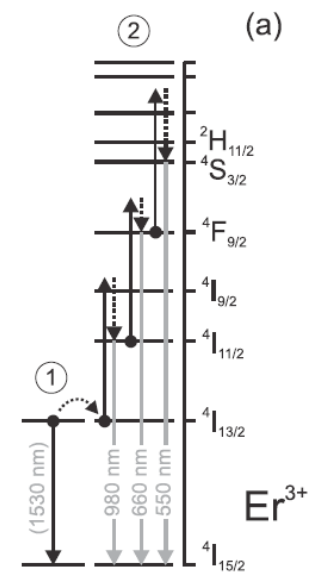


Fig. 1. (a) Energy level diagram of Er^{3+} ions. The black arrows depict the cooperative upconversion mechanism which causes the excitation of higher energy levels by energy upconversion of the end of a fabricated, tapered Au film. The scale bar is 1 μm .

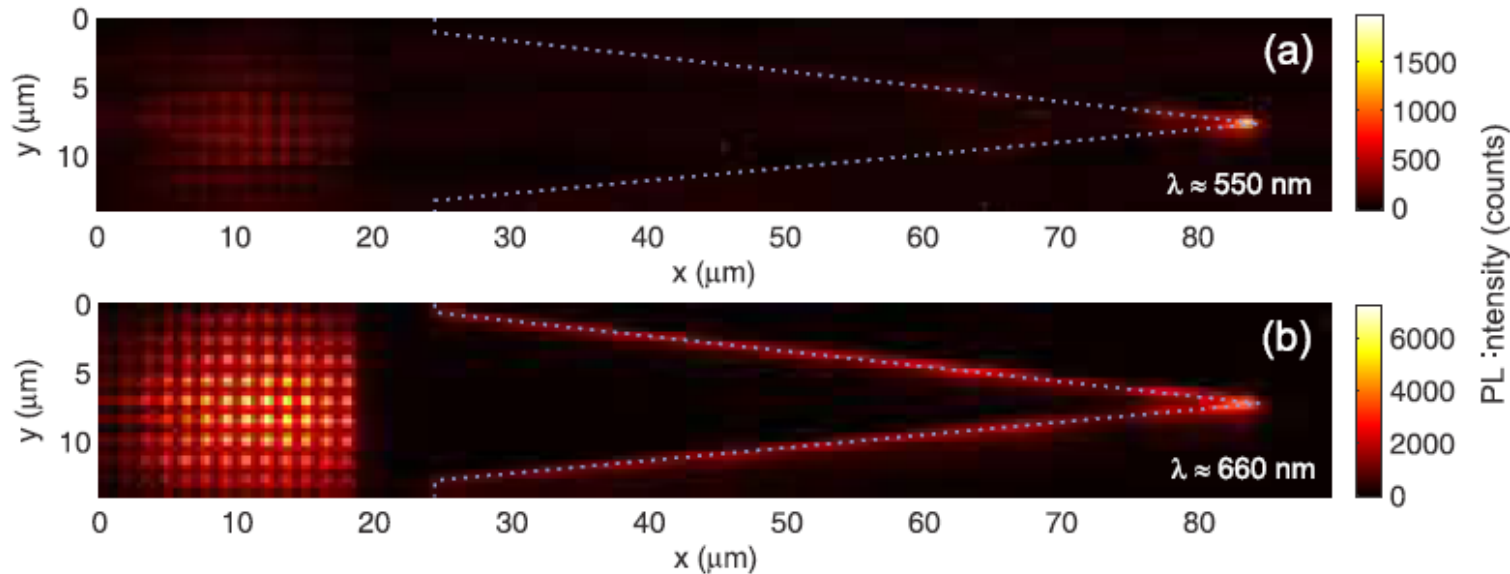


Fig. 5. Upconversion luminescence images taken from the air side of the film at (a) 550 nm and (b) 660 nm. The edge of the taper is indicated by the dotted line. Upconversion luminescence excited by SPPs on the substrate side of the film is observed from the edges of the taper, and the maximum intensity is detected at the taper tip.

Nanowire Plasmon Excitation by Adiabatic Mode Transformation

Ewold Verhagen,* Marko Spasenović, Albert Polman, and L. (Kobus) Kuipers
*Center for Nanophotonics, FOM Institute for Atomic and Molecular Physics (AMOLF),
Science Park 113, 1098 XG, Amsterdam, The Netherlands*

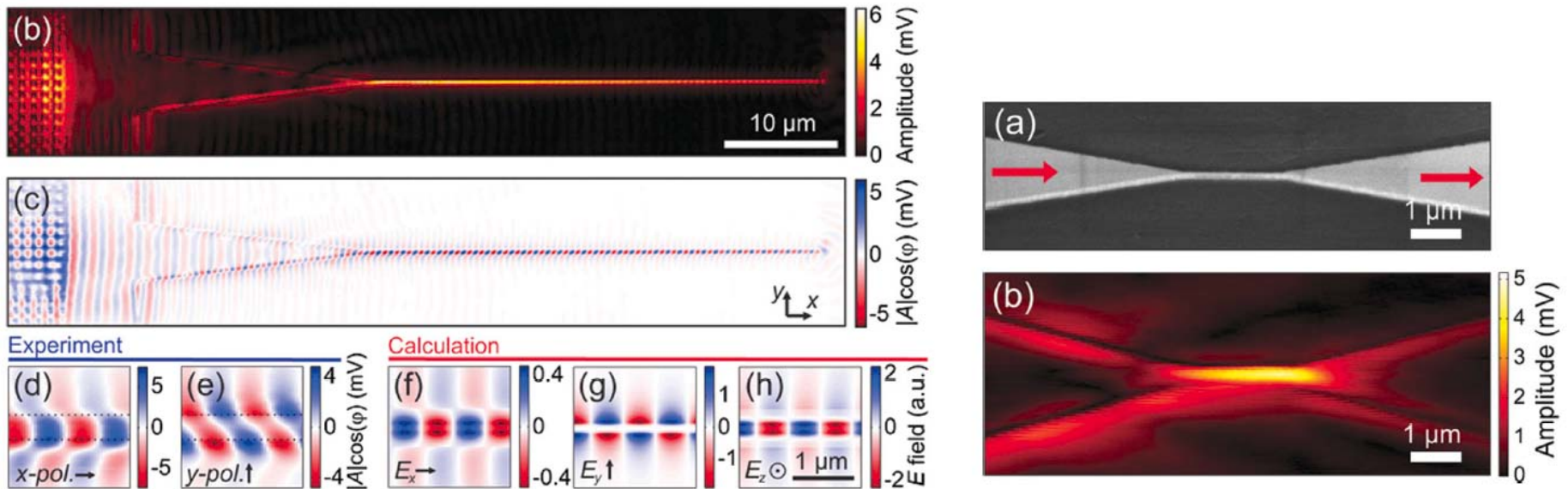


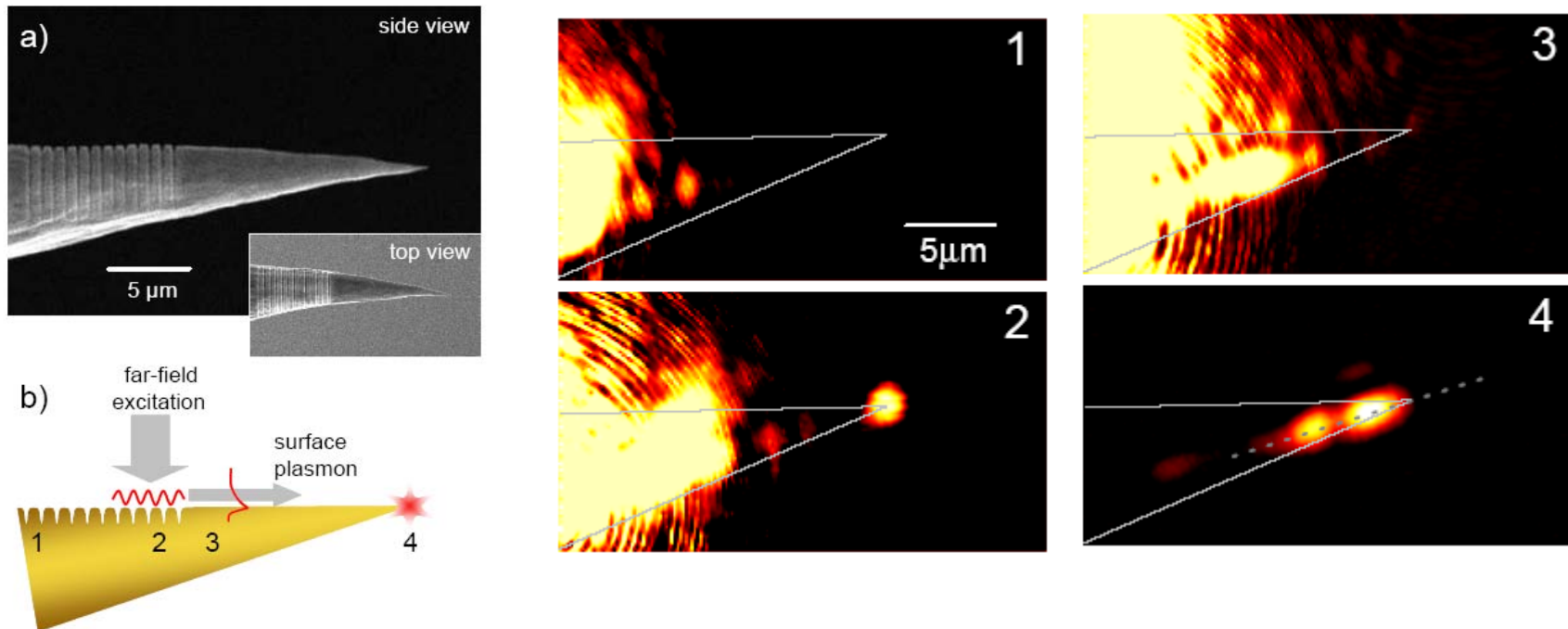
FIG. 4 (color). (a) Secondary electron micrograph of a $2 \mu\text{m}$ long nanowire connected by tapered waveguide sections for input and output coupling. (b) Near-field amplitude of forward-propagating waves in the structure at $\lambda = 1550 \text{ nm}$. The intensity transmission of the complete structure is $20 \pm 6\%$.

Grating-coupling of surface plasmons onto metallic tips: A nano-confined light source

Nano Lett. **7**, 2784-2788 (2007).

C. Ropers^{1,*}, C. C. Neacsu^{1,2}, T. Elsaesser¹, M. Albrecht³,
 M. B. Raschke^{1,2}, and C. Lienau⁴

¹Max-Born-Institut für Nichtlineare Optik und Kurzzeitspektroskopie,
 D-12489 Berlin, Germany



Near-Field Localization in Plasmonic Superfocusing: A Nanoemitter on a Tip

DOI: 10.1021/nl903574a | Nano Lett. 2010, 10, 592-596

Catalin C. Neacsu,^{†,‡} Samuel Berweger,^{†,‡} Robert L. Olmon,^{†,‡,§} Laxmikant V. Saraf,^{||} Claus Ropers,[⊥] and Markus B. Raschke^{*,†,§}

[†]Department of Chemistry, [‡]Department of Electrical Engineering, [§]Department of Physics, University of Washington, Seattle, Washington 98195
Laboratory, Richland, Washington 9935
University of Göttingen, Germany

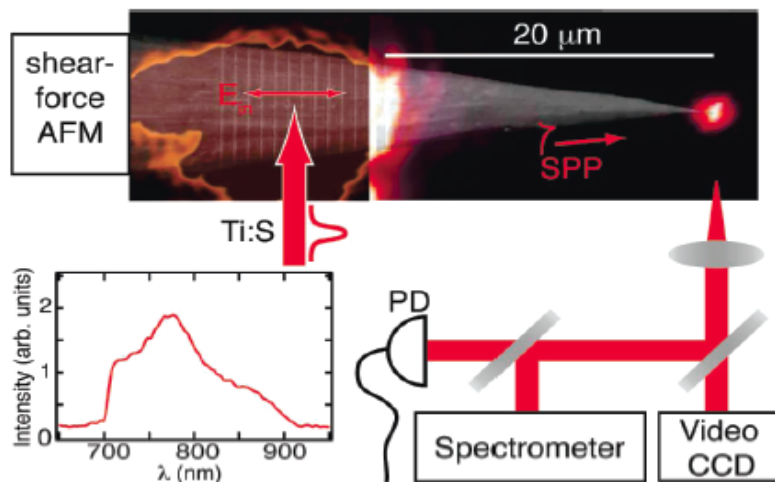


FIGURE 1. Grating coupling of surface plasmons on a tip. Overlay of SEM and optical far-field image of a Au tip with grating written by FIB for surface plasmon coupling of incident near-IR light from a Ti:Sapphire laser (spectrum shown). The grating with period $a_0 \sim 770$ nm is illuminated with polarization parallel with respect to the tip axis and an incident focus size of $\sim 8 \mu\text{m}$. The nonradiative SPP propagation leads to energy transfer and focusing and finally reemission near the tip apex with radius $\lesssim 15$ nm.

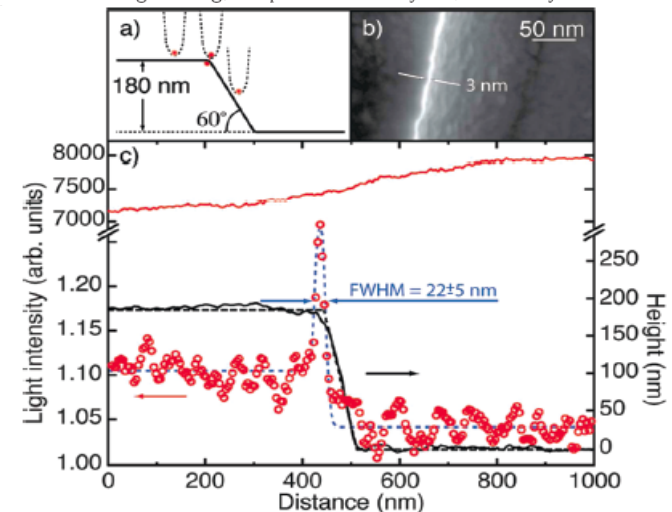


FIGURE 3. Determination of tip emitter size. (a) Schematic of scanning the nanofocusing tip across a silicon step edge with radius 3 ± 1 nm. (b) Top view SEM image of step edge. The wall and lower terrace are on the right-hand side. The edge serves as a local scatterer of the optical near-field of the apex. (c) The optical signal of a lateral scan across the step edge provides a measure of the spatial field confinement and thus the emitter size at the apex. Solid black line: AFM topography of the step. Red circles: plasmonic edge-scattered light intensity of the apex. The optical intensity peaks at the step edge and displays a width of 22 ± 5 nm, demonstrating the near-field localization at the apex. Solid red: Signal obtained under direct illumination of the apex under otherwise identical conditions.

Adiabatic Nanofocusing Scattering-Type Optical Nanoscopy of Individual Gold Nanoparticles

Diyar Sadiq,[†] Javid Shirdel,[†] Jae Sung Lee,[‡] Elena Selishcheva,[†] Namkyoo Park,[‡] and Christoph Lienau^{*,†}

[†]Institut für Physik, Carl von Ossietzky Universität, 26111 Oldenburg, Germany

[‡]Photonic Systems Laboratory, School of EECS, Seoul National University, Seoul 151-744, Korea

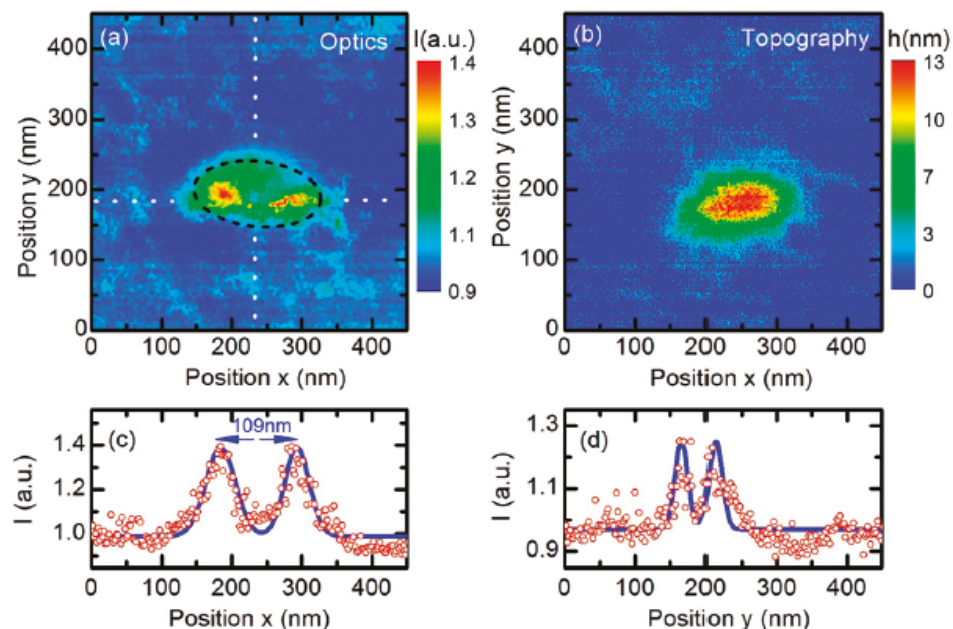
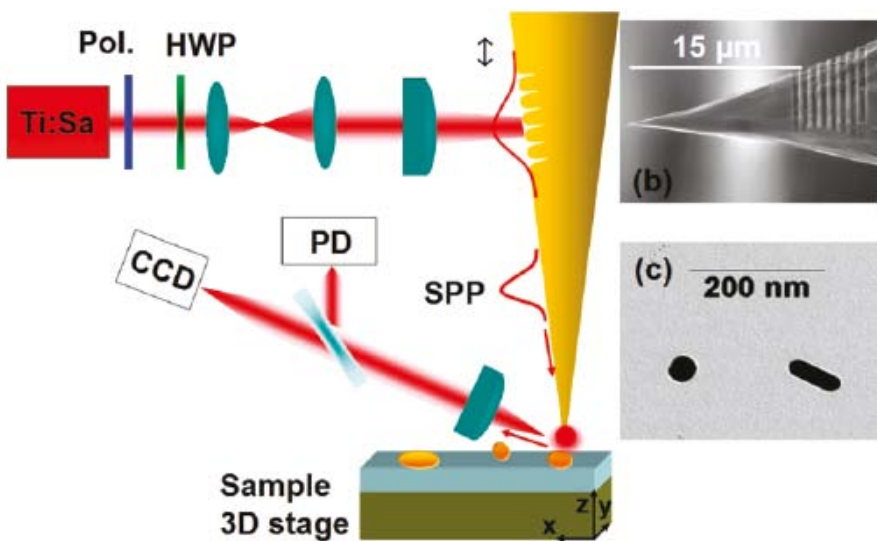
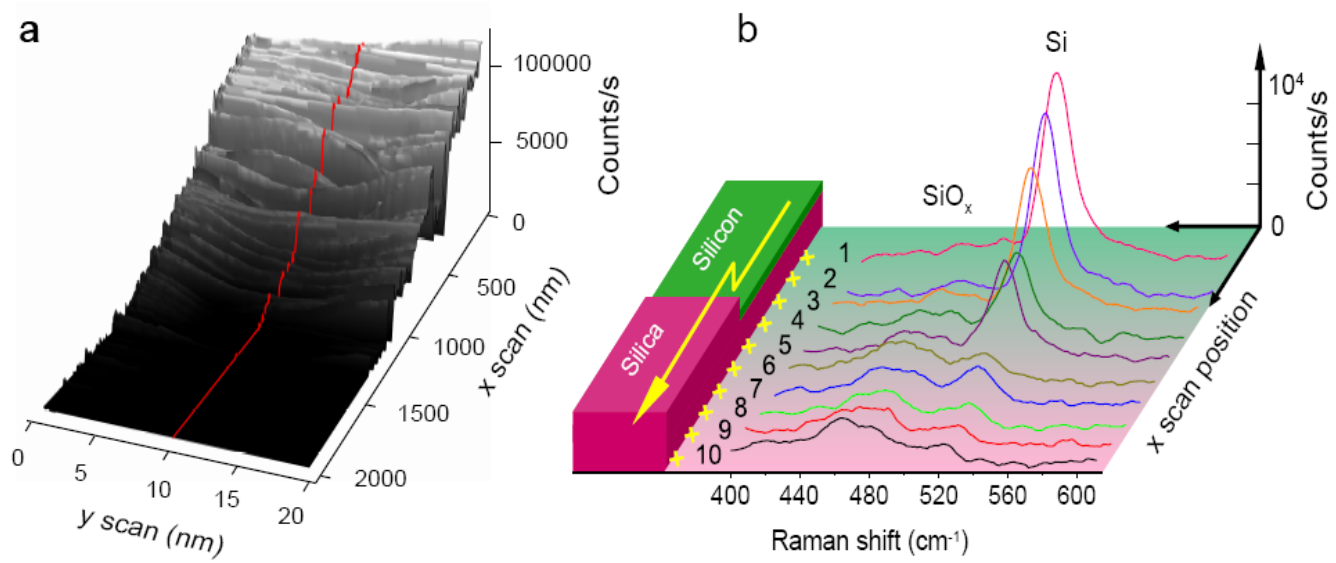
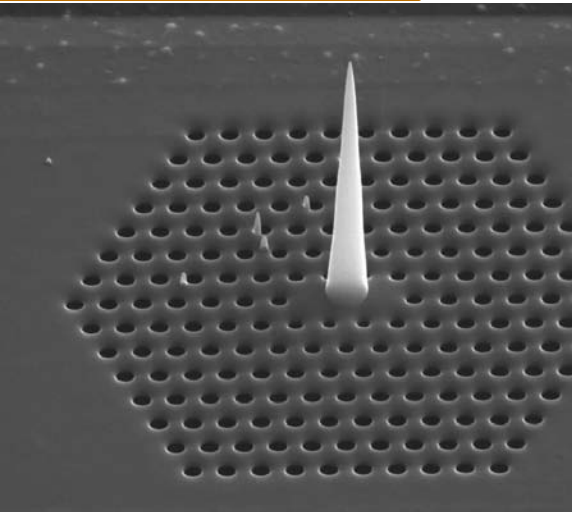


Figure 3. (a) Two-dimensional adiabatically focused s-NSOM image of an elliptical gold nanoparticle with $100 \times 40 \times 15 \text{ nm}^3$ dimensions on a glass substrate. (b) Corresponding shear-force topographical image of the elliptical gold nanoparticle. (c,d) Cross sections of the optical intensity along the x - and y -directions (along the dashed lines in panel a). The strong near-field enhancement at the edges of both the long and short axis of the nanoparticle indicates that the component of the local electric field oriented along the tip axis (z -direction) is imaged.

Di Fabrizio, E., *et. al*, Italian patent n. TO2008A000693 23.09.2008

5 nm radius



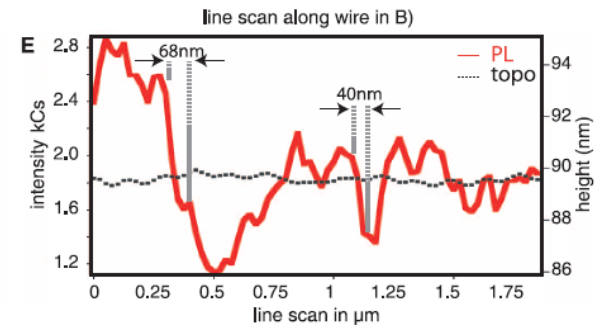
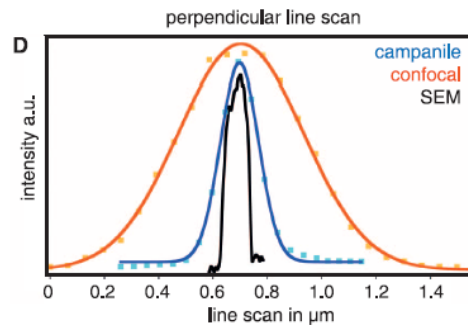
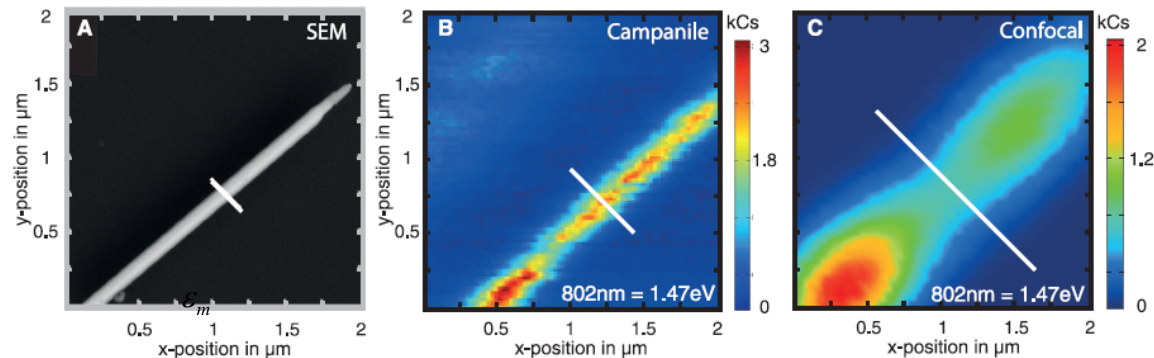
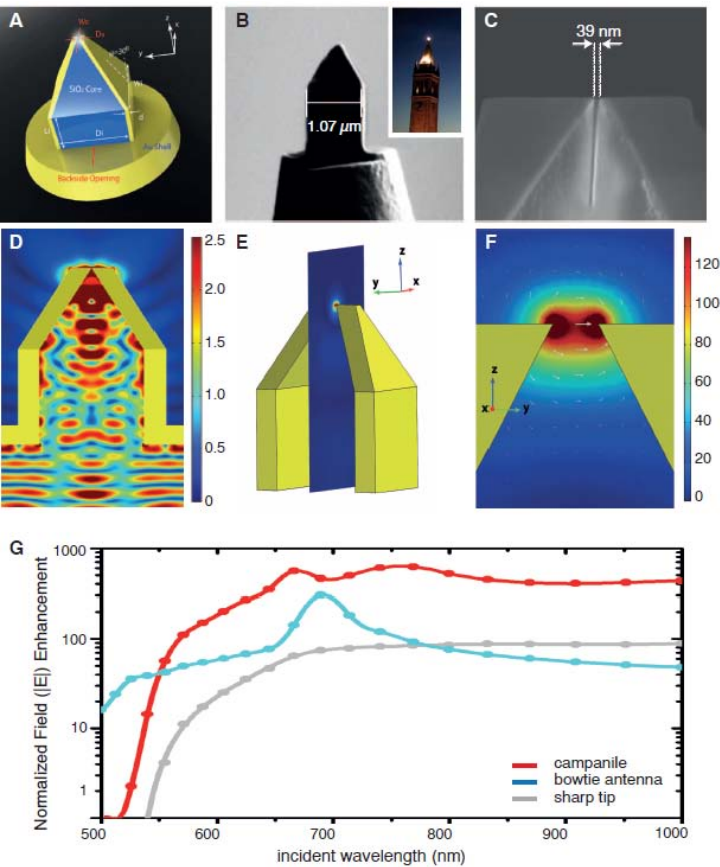
nature nanotechnology ARTICLES
 PUBLISHED ONLINE: 22 NOVEMBER 2009 | DOI: 10.1038/NNANO.2009.348

Nanoscale chemical mapping using three-dimensional adiabatic compression of surface plasmon polaritons

Francesco De Angelis^{1,2}, Gobind Das¹, Patrizio Candeloro², Maddalena Patrin³, Matteo Gall³, Alpan Bek⁴, Marco Lazzarino^{4,5}, Ivan Maksymov³, Carlo Liberale², Lucio Claudio Andreani³ and Enzo Di Fabrizio^{1,2*}

Mapping Local Charge Recombination Heterogeneity by Multidimensional Nanospectroscopic Imaging

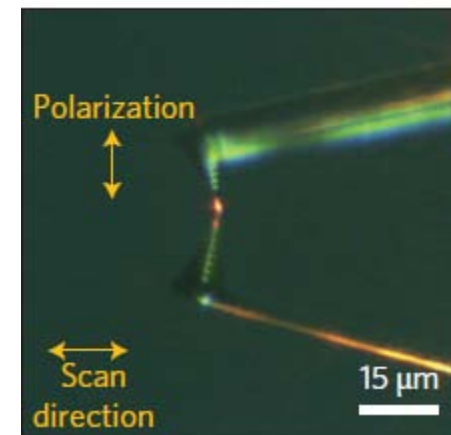
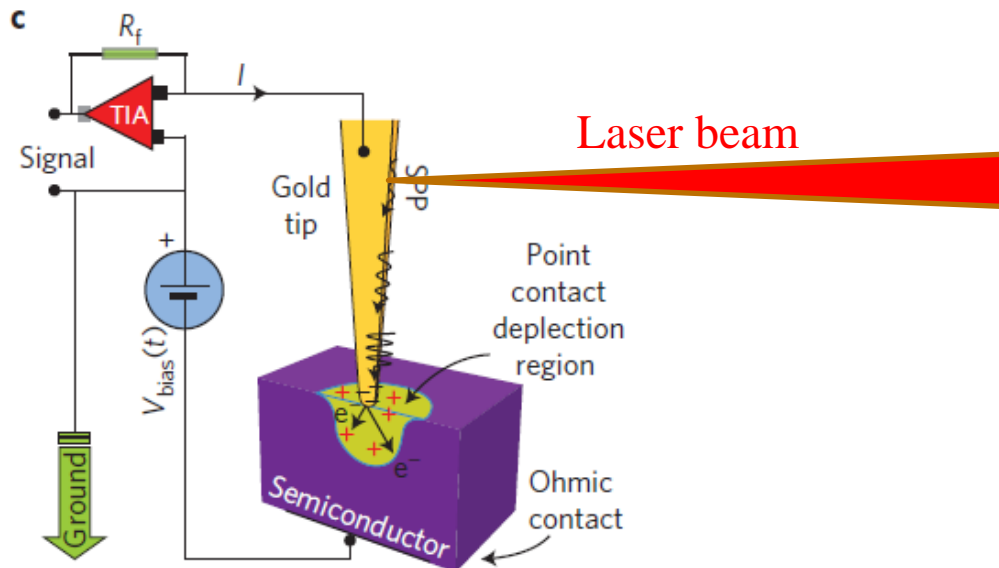
Wei Bao,^{1,2*} M. Melli,^{1*} N. Caselli,^{3,4} F. Riboli,^{3,4} D. S. Wiersma,^{3,5} M. Staffaroni,⁶ H. Choo,⁷ D. F. Ogletree,¹ S. Aloni,¹ J. Bokor,^{1,6} S. Cabrini,^{1,†} F. Intonti,^{3,4} M. B. Salmeron,^{1,2} E. Yablonovitch,⁶ P. J. Schuck,^{1,†} A. Weber-Bargioni^{1,†}



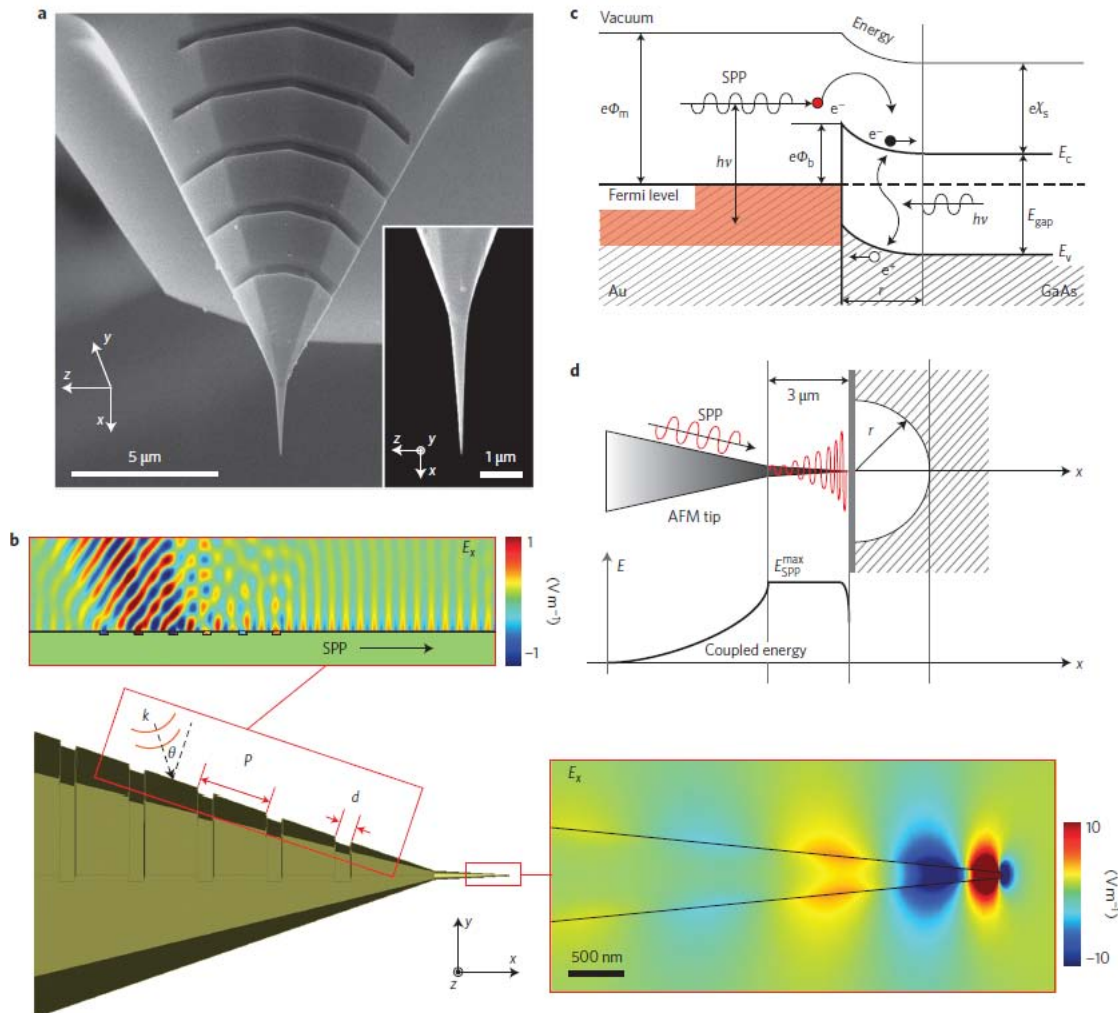
Hot-electron nanoscopy using adiabatic compression of surface plasmons

A. Giugni^{1,2}, B. Torre^{2,3}, A. Toma¹, M. Francardi^{2,4}, M. Malerba¹, A. Alabastri¹, R. Proietti Zaccaria¹, M. I. Stockman^{5,6,7} and E. Di Fabrizio^{2,4*}

Surface plasmon polaritons propagate along the adiabatic plasmonic taper, nanofocus at the tip, and decay due to Landau damping, producing a nanosource of hot electrons at the tip, which forms a Schottky diode with the substrate



Geometry and principle of adiabatic-plasmonic hot-electron Schottky nanoscopy



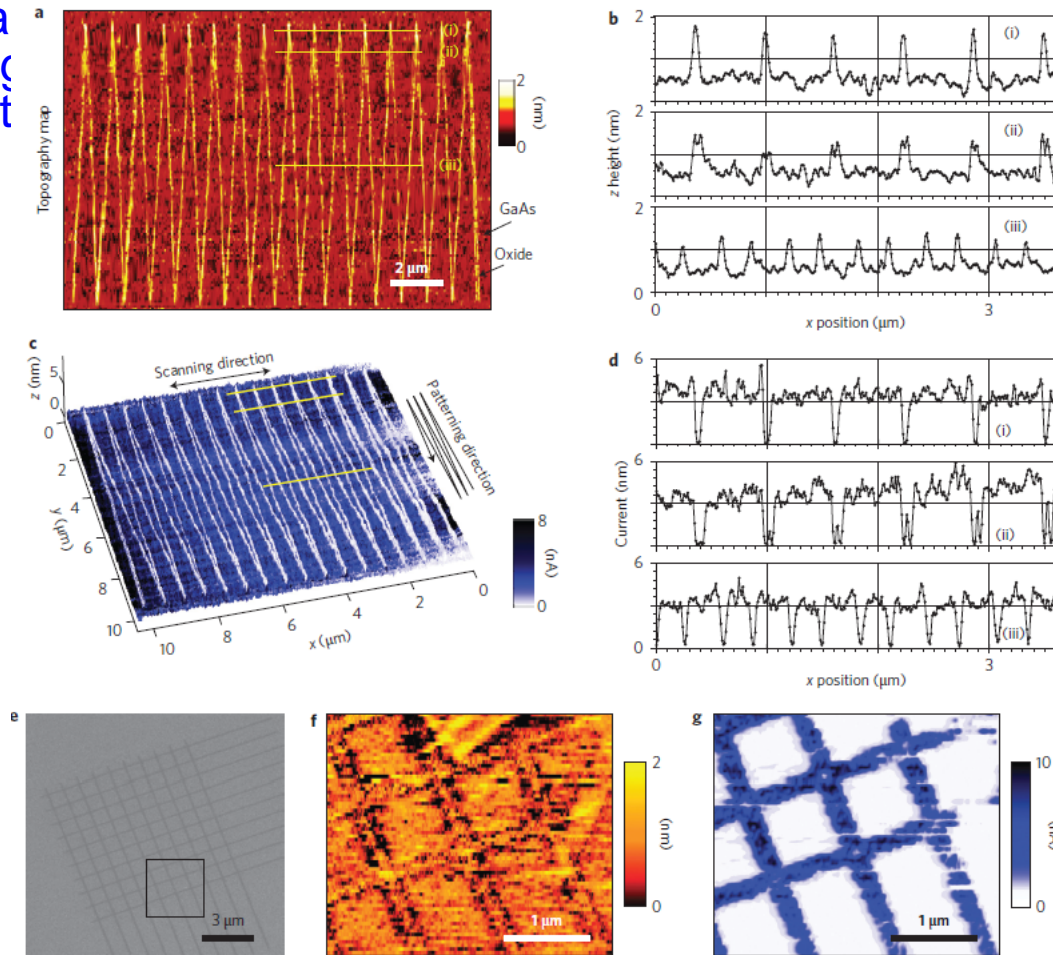
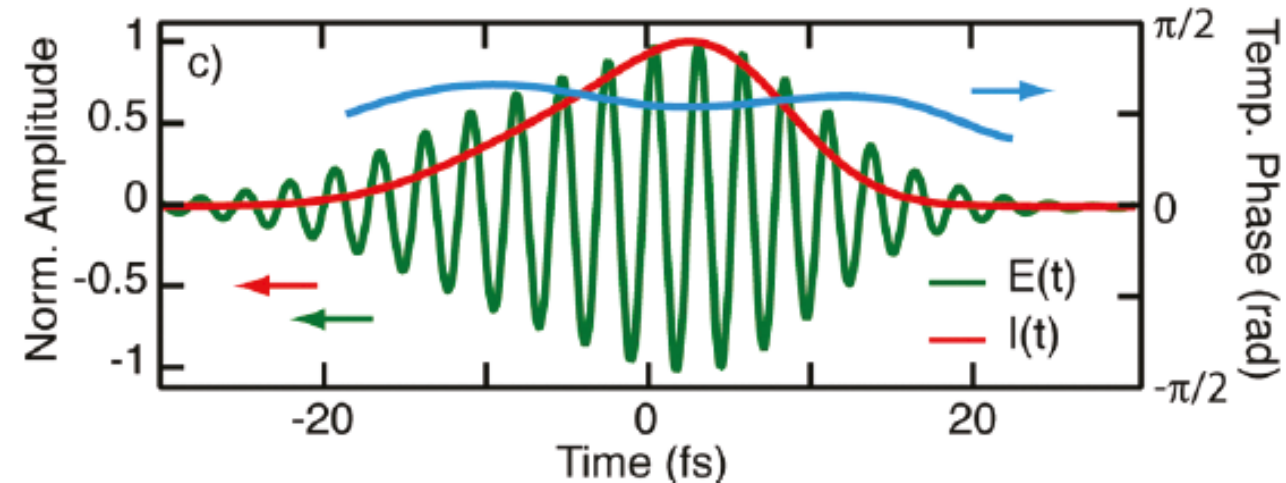
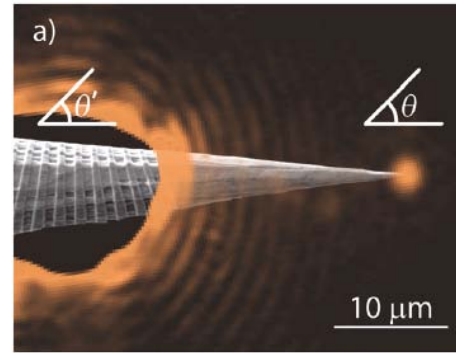
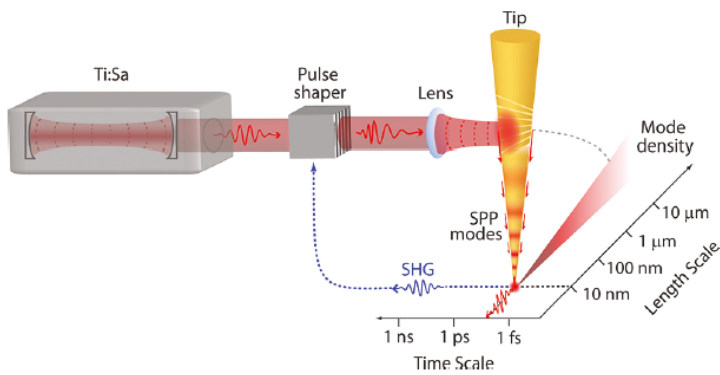


Figure 5 | Three-dimensional hot-electron maps of specific custom-realized locally patterned samples. Topography and photocurrent maps show both locally oxidized surfaces and ion-implanted conductive samples, respectively excited at λ_1 and λ_2 . **a,b**, High-resolution AFM topography and height profiles of a continuous oxide pattern deposited on GaAs made by a top-down fabrication technique through high field discharge in water ($\sim 40\%$ ambient air humidity). The pattern was written using the same plasmonic tip with $+4$ V sample bias at $4 \mu\text{m s}^{-1}$ writing speed, in contact mode (set point 10 nN). Topography map and profiles (indicated by yellow lines in the map) are not deconvolved for the tip profile. **c**, Photocurrent imaging overlaid on three-dimensional topography, showing simultaneously the achieved current and topographic resolution. **d**, Single line photocurrent intensity profiles indicated with a yellow line on image **c**. The photocurrent measure was performed by scanning in AFM contact mode with a 90° angle to the patterned surface, under a N_2 atmosphere. The zigzag profile allows a direct check of experimental resolutions from line profiles (ii) of **b** and **d**. **e**, SEM image of Ga ion-implanted GaAs sample. **f,g**, Topography and plasmonic hot-electron maps, generated at 980-nm laser excitation, acquired in the region indicated by a black rectangle in **e**. The pattern was fabricated by a focused ion beam process as single grid lines (40 pA , $100 \text{ ns point}^{-1}$, 30 keV , single pass).

Femtosecond Nanofocusing with Full Optical Waveform Control

Samuel Berweger,[†] Joanna M. Atkin,[†] Xiaoji G. Xu, Robert L. Olmon, and Markus B. Raschke*

Department of Physics, Department of Chemistry, and JILA, University of Colorado at Boulder, Boulder, Colorado 80309, United States



Nearly transform-limited 16-fs pulse at the apex

Adiabatic Nanofocusing Conclusions

- Due to adiabaticity, the back reflection and 3D scattering of SPP is minimal.
- The high wave vector of the TM₀ SPP makes them dark (no coupling to the far field radiation).
- The velocity of SPP tends to zero proportionally to R as they approach the tip: *adiabatic slowing down and asymptotic stopping*.
- This leads to the accumulation of the SPP near the tip and their *adiabatic nanofocusing*.
- Under realistic conditions it is possible to transfer to the tip vicinity ~50% of the initial energy flux, that along with adiabatic stopping leads to the local field-intensity enhancement by three orders of magnitude
- The energy and optical field concentration at the tip of a taper is usable to excite a high-sensitivity, low-background SERS from a few molecules

A dramatic sunset over a body of water. The sky is filled with dark, heavy clouds, with a bright orange and red glow from the setting sun breaking through. In the foreground, the dark silhouettes of buildings are visible. The water is dark, and many small sailboats are scattered across the horizon. The overall mood is serene and atmospheric.

END LECTURE 1